

## Supporting Information

### **Systemic regulation of binding sites in porous coordination polymers for ethylene purification from ternary C<sub>2</sub> hydrocarbons**

Yi Li,<sup>a</sup> Yanxin Wu,<sup>a</sup> Jiabin Zhao,<sup>a</sup> Jingui Duan<sup>a, b, \*</sup> Wanqin Jin<sup>a, \*</sup>

<sup>a</sup> State Key Laboratory of Materials-Oriented Chemical Engineering, College of Chemical Engineering, Nanjing Tech University, Nanjing 211816, China.

<sup>b</sup> State Key Laboratory of Chemistry and Utilization of Carbon Based Energy Resources, College of Chemistry, Xinjiang University, Urumqi, 830017, China.

Email: [duanjingui@njtech.edu.cn](mailto:duanjingui@njtech.edu.cn) (J.D.); [wqjin@njtech.edu.cn](mailto:wqjin@njtech.edu.cn) (W. J.)

## General procedures and materials

All the solvents and materials were purchased from chemical vendors and without further depuration before used. The instrument used for the  $^1\text{H}$  NMR test was a Bruker Advance III 600 MHz nuclear magnetic resonance spectrometer Powder X-Ray Diffraction (PXRD) pattern was tested with Rigaku SmartLab (test conditions: 40 kV, 40 mA,  $\text{CuK}\alpha$ ,  $\lambda = 1.5418 \text{ \AA}$ , scanning range  $5\text{-}30^\circ$ ). Infrared (FT-IR) spectra were tested on the VECTOR 22 spectrometer using KBr tableting method in the range of  $4000\text{-}400 \text{ cm}^{-1}$ . Thermogravimetric analysis (TGA) measurements were performed on a STA 209 F1 instrument under astatic  $\text{N}_2$  atmosphere with a heating rate of  $5 \text{ }^\circ\text{C}/\text{min}$  at the range of  $50\text{-}700 \text{ }^\circ\text{C}$ . Raman spectra of gas loaded samples were collected on a Horiba Jobin-Yvon HR800 Raman Spectrometer at 298 K.

## Ligand synthesis

**L1** was prepared according to our previous work.<sup>1</sup>

**L2**: A mixture of 3,5-dibromo-trifluoromethylbenzene (5.14 g, 16.9 mmol), imidazole (4.86 g, 71.4 mmol),  $\text{K}_2\text{CO}_3$  (7.4 g, 53.5 mmol) and  $\text{CuSO}_4$  (0.05 g, 0.35 mmol) were mixed in a Teflon-lined autoclave under  $\text{N}_2$  atmosphere and heated to  $180 \text{ }^\circ\text{C}$  and kept for 72 h. After cooling down, the crude product was solved in water (100 mL) and then extracted with dichloromethane for three times ( $3 \times 50 \text{ mL}$ ). The organic phase was combined and washed three times with water ( $3 \times 20 \text{ mL}$ ). **L2** was obtained as a pale-yellow solid (Yield:  $\sim 86\%$ ).  $^1\text{H}$  NMR ( $\text{DMSO-}d_6$ ) of **L2**:  $\delta = 7.18$  (2H, s), 8.07 (4H, s), 8.30 (1H, s), 8.57 (2H, s).

**L3**: A mixture of 1,3-dibromo-5-methylbenzene (4.22 g, 16.9 mmol), imidazole (4.86 g, 71.4 mmol),  $\text{K}_2\text{CO}_3$  (7.4 g, 53.5 mmol) and  $\text{CuSO}_4$  (0.05 g, 0.35 mmol) were mixed in a Teflon-lined autoclave under  $\text{N}_2$  atmosphere and heated to  $180 \text{ }^\circ\text{C}$  and kept for 72 h. After cooling down, the crude product was solved in water (100 mL) and then extracted with dichloromethane for three times ( $3 \times 50 \text{ mL}$ ). The organic phase was combined and washed three times with water ( $3 \times 20 \text{ mL}$ ). **L3** was obtained as a pale-yellow solid (Yield:  $\sim 92\%$ ).  $^1\text{H}$  NMR ( $\text{DMSO-}d_6$ ) of **L3**:  $\delta = 2.44$  (3H, s), 7.13 (2H, s), 7.51 (2H, s), 7.79 (1H, s), 7.88 (2H, s), 8.40 (2H, s).

## Crystal analysis

Single-crystal X-ray diffraction data was collected by Rigaku XtaLAB Synergy diffractometer at room temperature using graphite monochromator  $\text{Mo K}\alpha$  radiation ( $\lambda = 0.71073 \text{ \AA}$ ). Data reduction was made with the Saint program. Empirical absorption correction using spherical harmonics, implemented in SCALE3 ABSPACK scaling algorithm. The structure was solved by direct methods and refined with full-matrix least-squares technique using the SHELXTL package.<sup>2</sup> Non-hydrogen atoms were refined with anisotropic displacement parameters during the final cycles. Organic hydrogen atoms were placed in calculated positions with isotropic displacement parameters set to  $1.2 \times U_{\text{eq}}$  of the attached atom. We have employed PLATON/SQUEEZE<sup>3, 4</sup> to calculate the diffraction contribution of the solvent molecules and, thereby, to produce a set of solvent-free diffraction intensities; structures were then refined again using the data generated. For the in-situ measurements, the fully activated **NTU-73-series** that loaded inside the half-open glass tube was purged with corresponding gas at 298 K with pressure of 1 bar, respectively. The tubes were then sealed with hot candle under the corresponding atmosphere. The single crystal measurements were performed on a Rigaku XtaLAB Synergy diffractometer at room temperature. Crystal data are summarized in Table S1 and S5.

### Sample activation

Prior to adsorption measurement, the samples were prepared by immersing the as-synthesized samples in dry acetone (**NTU-73-COOH**) or methanol (**NTU-73-CF<sub>3</sub>** and **NTU-73-CH<sub>3</sub>**) for three days to remove non-volatile solvents, and the extract was decanted every 8 h and replaced with fresh solvent. The completely activated **NTU-73-COOH** was obtained by heating the solvent-exchanged samples at 30 °C under a dynamic high vacuum for 24 h, while the completely activated **NTU-73-CF<sub>3</sub>** and **NTU-73-CH<sub>3</sub>** were obtained by heating the solvent-exchanged samples at 30 °C (24 h) and then to 80 °C (12 h) under a dynamic high vacuum.

### In-situ Raman test

For the in-situ Raman test, the fully activated **NTU-73-CH<sub>3</sub>** that loaded inside the half-open glass tube was purged with He, C<sub>2</sub>H<sub>4</sub> or C<sub>2</sub>H<sub>6</sub> at 298 K, 1 bar, respectively. The tubes were then sealed with hot candle under the corresponding atmosphere. After that, Raman spectra of the gas-loaded **NTU-73-CH<sub>3</sub>** were then collected on a Horiba Jobin-Yvon HR800 Raman spectrometer at room temperature.

### Single gas adsorption

In the gas adsorption measurement, ultra-high-purity grade of N<sub>2</sub>, CO<sub>2</sub>, C<sub>2</sub>H<sub>2</sub>, C<sub>2</sub>H<sub>4</sub>, and C<sub>2</sub>H<sub>6</sub> gases were used throughout the adsorption experiments. Gas adsorption isotherms were collected using a Belsorp-mini volumetric adsorption instrument from BEL Japan Inc, using the volumetric technique.

### Estimation of the isosteric heats of gas adsorption

A virial-type expression comprising the temperature-independent parameters  $a_i$  and  $b_i$  was employed to calculate the enthalpies of adsorption for C<sub>2</sub>H<sub>2</sub>, C<sub>2</sub>H<sub>6</sub> and C<sub>2</sub>H<sub>4</sub> (at 273 K, 283 K and 298 K) on **NTU-73-COOH**, **NTU-73-CF<sub>3</sub>**, **NTU-73-CH<sub>3</sub>**. In each case, the data were fitted using the equation (1):

$$\ln P = \ln N + 1/T \sum_{i=0}^m a_i N^i + \sum_{i=0}^n b_i N^i \quad (1)$$

Here,  $P$  is the pressure expressed in Torr,  $N$  is the amount adsorbed in mmol g<sup>-1</sup>,  $T$  is the temperature in K,  $a_i$  and  $b_i$  are virial coefficients, and  $m$ ,  $n$  represent the number of coefficients required to adequately describe the isotherms ( $m$  and  $n$  were gradually increased until the contribution of extra added  $a$  and  $b$  coefficients was deemed to be statistically insignificant towards the overall fit, and the average value of the squared deviations from the experimental values was minimized).

$$Q_{st} = -R \sum_{i=0}^m a_i N^i \quad (2)$$

Here,  $Q_{st}$  is the coverage-dependent isosteric heat of adsorption and  $R$  is the universal gas constant (2).

### Selectivity prediction for binary mixture adsorption

Ideal adsorbed solution theory (IAST) was used to predict binary mixture adsorption from the experimental pure-gas isotherms. To perform the integrations required by IAST, the single-component isotherms should be fitted by a proper model. There is no restriction on the choice of the model to fit the adsorption isotherm, however, data over the pressure range under study should be fitted very precisely. Several isotherm models were tested to fit the experimental pure isotherms for C<sub>2</sub>H<sub>2</sub>, C<sub>2</sub>H<sub>6</sub> and C<sub>2</sub>H<sub>4</sub> of 1, and the dual-site Langmuir-Freundlich equation (3) were found to the best fit to the experimental data:

$$q = q_{m1} \cdot \frac{b_1 \cdot P^{1/n_1}}{1 + b_1 \cdot P^{1/n_1}} + q_{m2} \cdot \frac{b_2 \cdot P^{1/n_2}}{1 + b_2 \cdot P^{1/n_2}} \quad (3)$$

Here,  $P$  is the pressure of the bulk gas at equilibrium with the adsorbed phase (kPa),  $q$  is the adsorbed amount per mass of adsorbent (mol kg<sup>-1</sup>),  $q_{m1}$  and  $q_{m2}$  are the saturation capacities of sites 1 and 2 (mol kg<sup>-1</sup>),  $b_1$  and  $b_2$  are the affinity coefficients of the sites (1/kPa), and  $n_1$  and  $n_2$  are measures of the deviations from an ideal homogeneous surface. The  $R_2$  values for all of the fitted isotherms were over 0.99997. Hence, the fitted isotherm parameters were applied to perform the necessary integrations in IAST.

#### Stability test

Crystals of **NTU-73-COOH**, **NTU-73-CF<sub>3</sub>** and **NTU-73-CH<sub>3</sub>** were soaked in chemical solutions (pH = 2, pH = 7 and pH = 12) for 3 days or exposed in the air atmosphere for 7 days. After treatment, all crystals were examined by PXRD, only expect partial **NTU-73-CH<sub>3</sub>** crystals were activated for gas adsorption measurements.

#### Breakthrough measurements

The breakthrough experiments were performed on the Beifang Gaorui CT-4 system. Mass flow controllers regulate the flow rates of all gases. Effluent gas stream from the column is monitored by gas chromatography detector. The initial activated **NTU-73-COOH** (2.0189 g), **NTU-73-CF<sub>3</sub>** (2.4984 g) and **NTU-73-CH<sub>3</sub>** (2.9962 g) crystals were packed into a stainless-steel column ( $\varphi = 3$  mm,  $L = 20$  cm) tightly. All samples were activated at 30 °C under a dynamic high vacuum for 72 hours. Then, helium flow was introduced into the system for pressure compensation and then the feed gas was changed to C<sub>2</sub>H<sub>2</sub>/C<sub>2</sub>H<sub>4</sub>, C<sub>2</sub>H<sub>6</sub>/C<sub>2</sub>H<sub>4</sub> or C<sub>2</sub>H<sub>2</sub>/C<sub>2</sub>H<sub>6</sub>/C<sub>2</sub>H<sub>4</sub> mixtures. System pressure was monitored by pressure sensors.

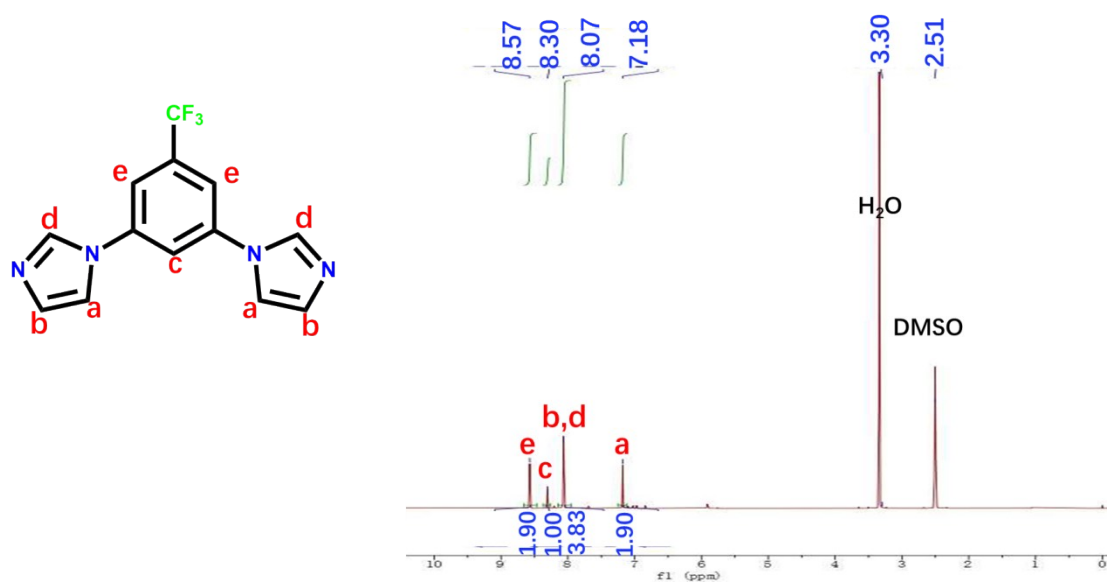


Figure S1. <sup>1</sup>H NMR spectrogram of L2.

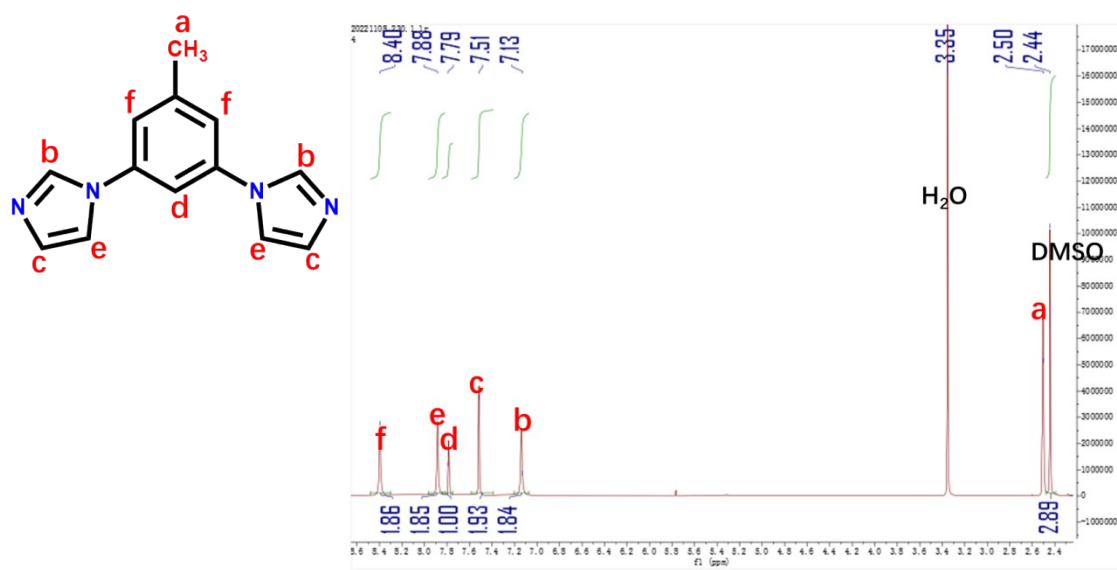
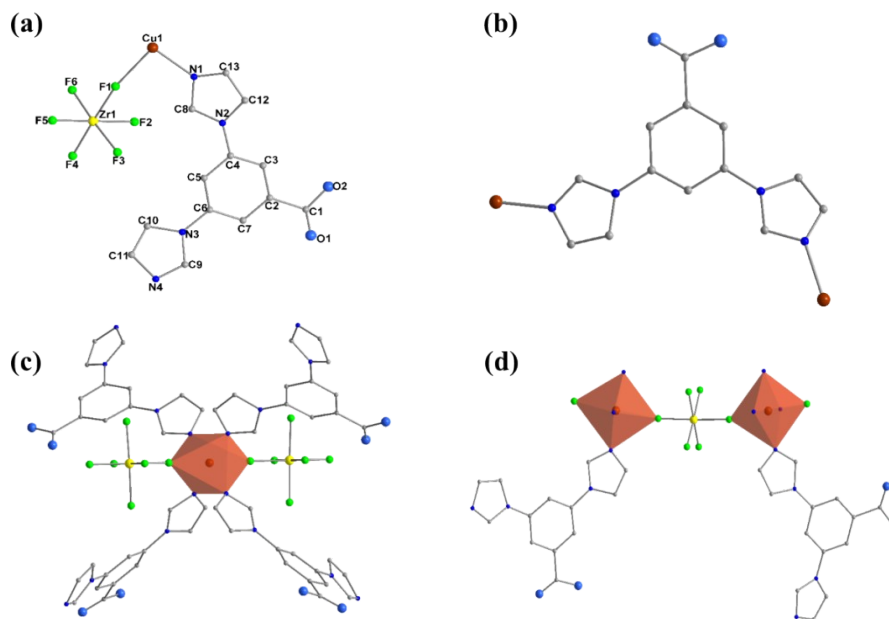
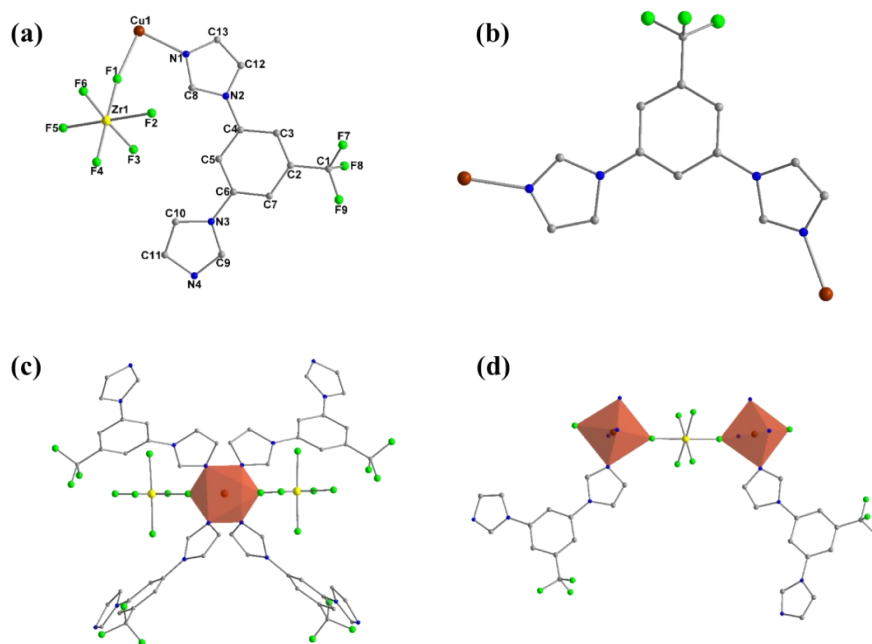


Figure S2. <sup>1</sup>H NMR spectrogram of L3.



**Figure S3.** Structure of **NTU-73-COOH**: Asymmetric unit (a); Ligand connection (b); Coordination configuration of Cu center (c) and  $ZrF_6^{2-}$  ion connection (d).



**Figure S4.** Structure of **NTU-73-CF<sub>3</sub>**: Asymmetric unit (a); Ligand connection (b); Coordination configuration of Cu center (c) and  $ZrF_6^{2-}$  ion connection (d).

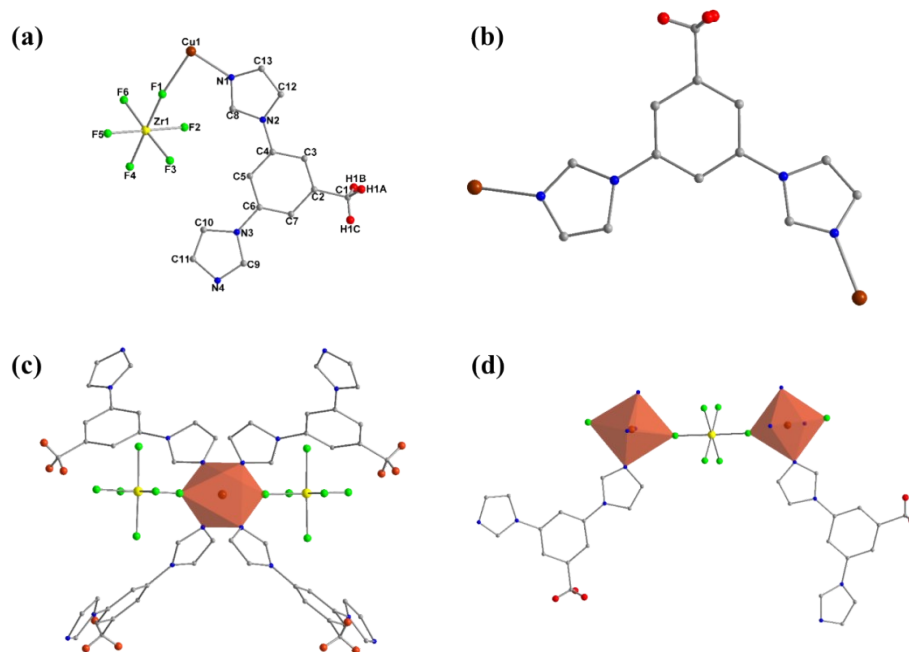


**Figure S5.** Structure of **NTU-73-CH<sub>3</sub>**: Asymmetric unit (a); Ligand connection (b); Coordination configuration of Cu center (c) and ZrF<sub>6</sub><sup>2-</sup> ion connection (d).

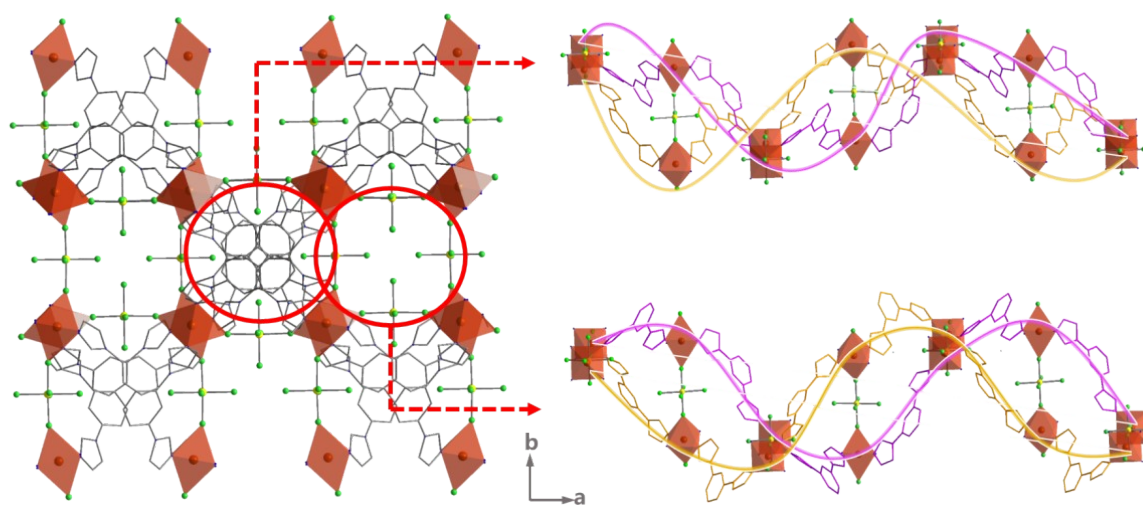


**Figure S6.** Two helix chains in **NTU-73-COOH**.

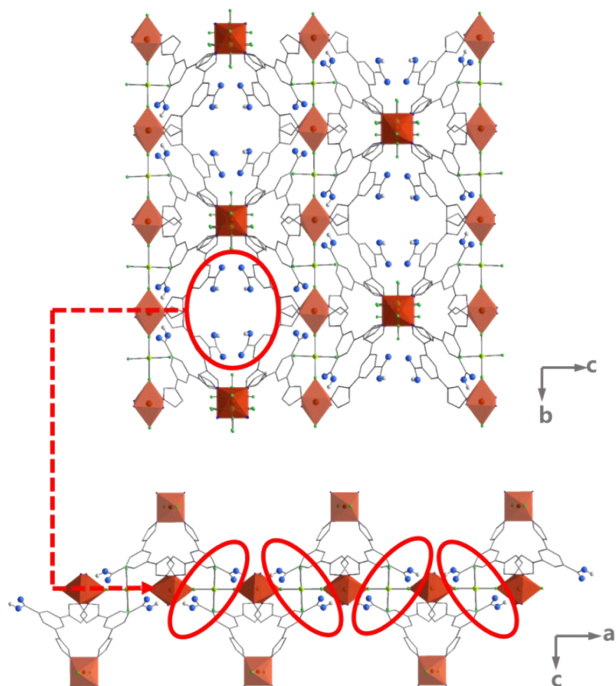


**Figure S7.** View of the carboxylic pincers that packed alternatively in **NTU-73-COOH** along b-axis.

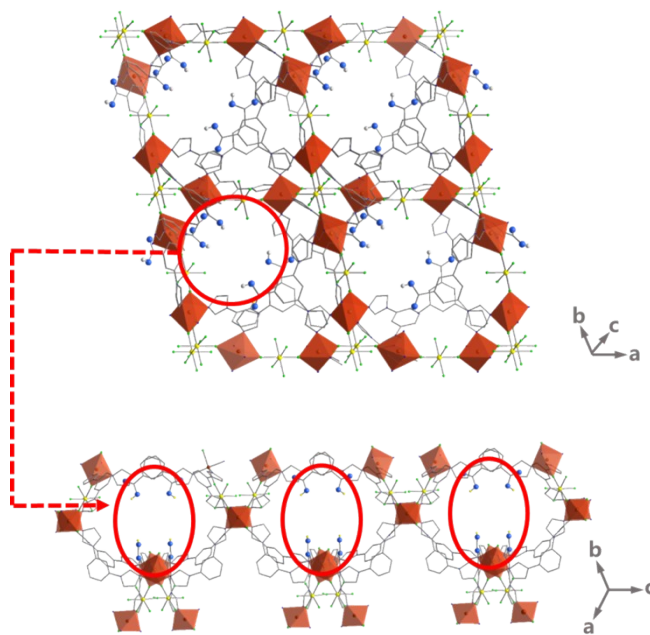


**Figure S8.** View of the carboxylic pincers that packed alternatively in **NTU-73-COOH** along another direction.

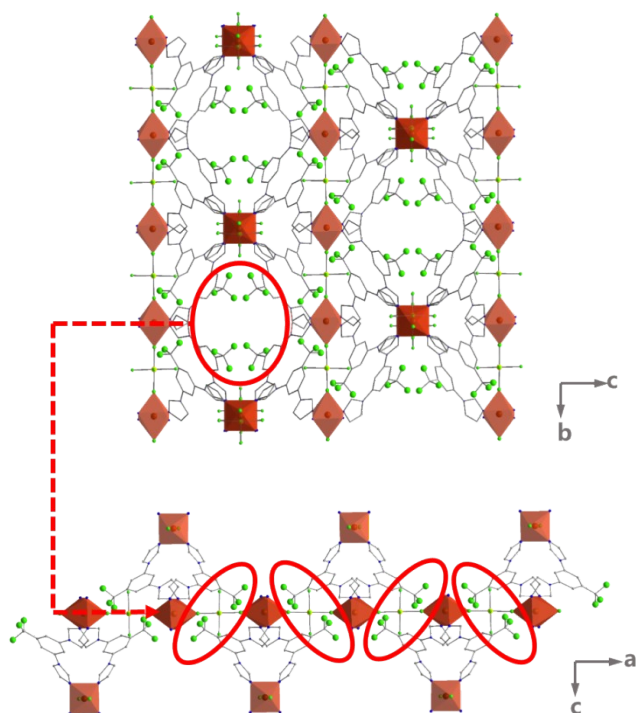


**Figure S9.** View of the  $-\text{CF}_3$  sites that packed alternatively in **NTU-73-CF<sub>3</sub>** along b-axis.

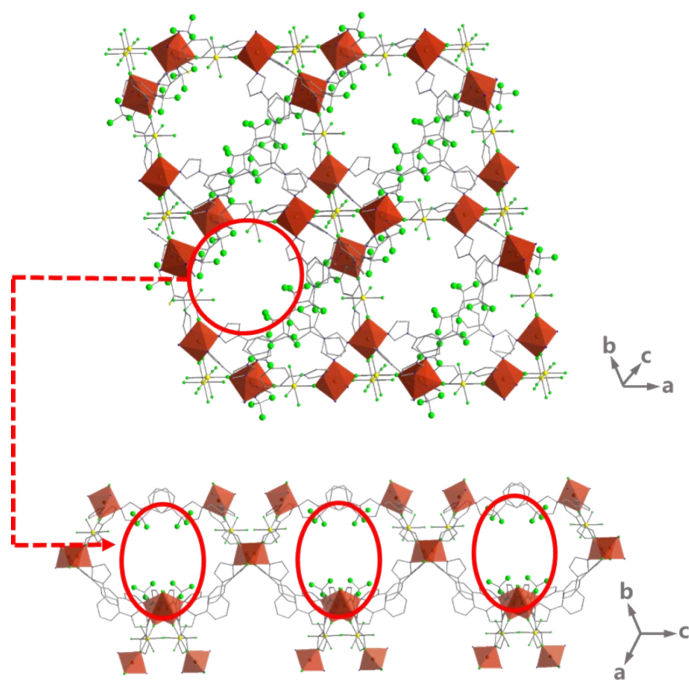


**Figure S10.** View of the  $-\text{CF}_3$  sites that packed alternatively in **NTU-73-CF<sub>3</sub>** along another direction.

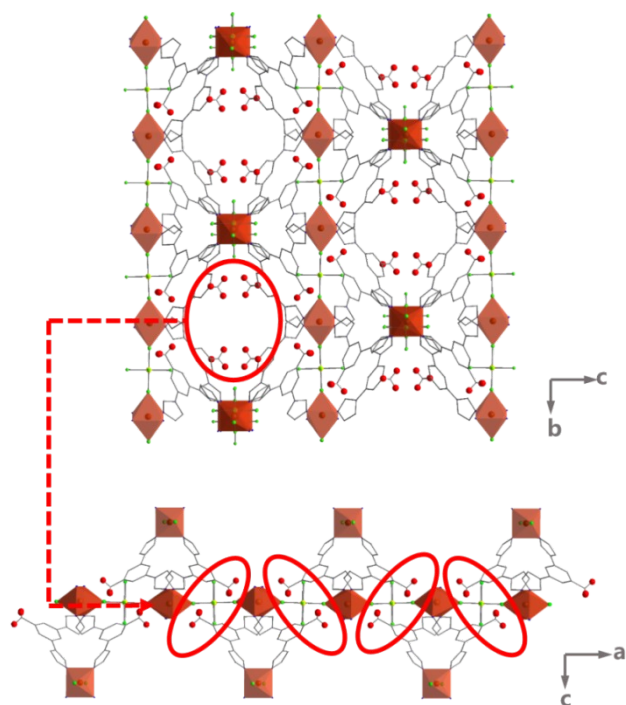


**Figure S11.** View of the  $-\text{CH}_3$  sites that packed alternatively in **NTU-73- $\text{CH}_3$**  along b-axis.

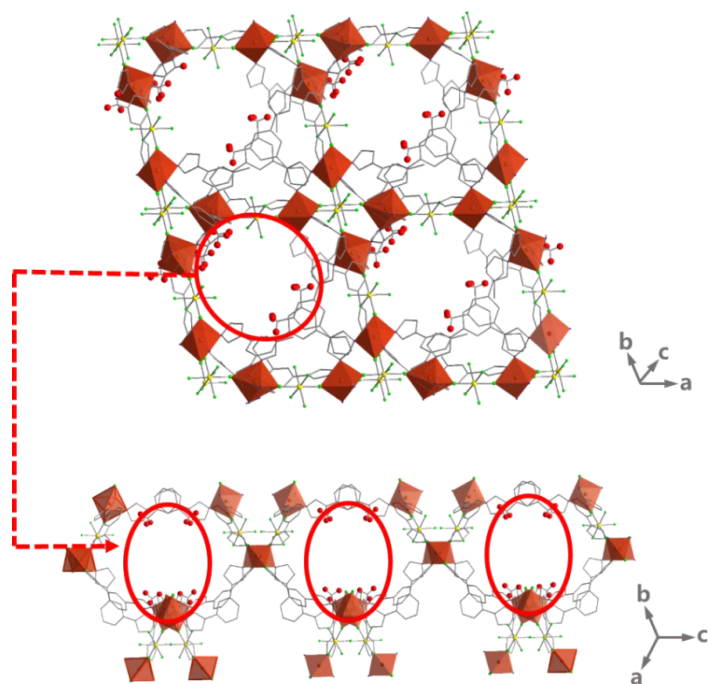


**Figure S12.** View of the  $-\text{CH}_3$  sites that packed alternatively in **NTU-73- $\text{CF}_3$**  along another direction.

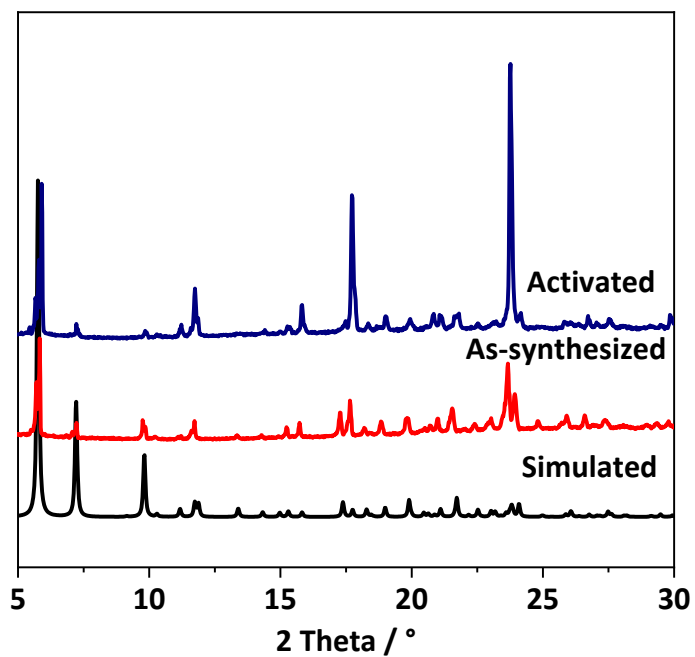


Figure S13. PXRD patterns of NTU-73-COOH.

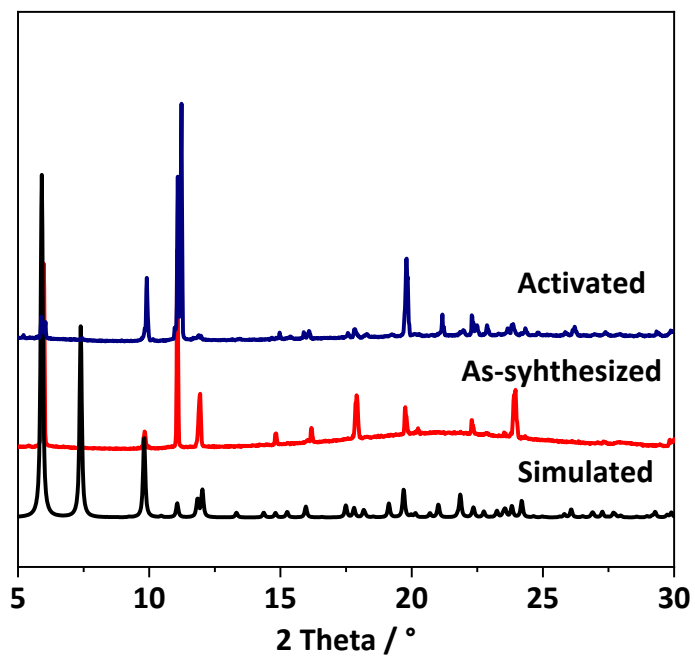


Figure S14. PXRD patterns of NTU-73-CF<sub>3</sub>.

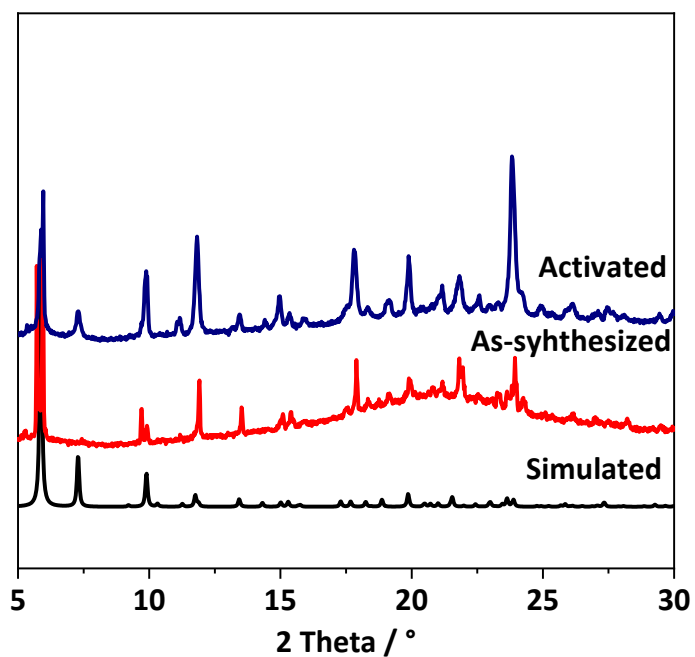


Figure S15. PXRD patterns of NTU-73-CH<sub>3</sub>.

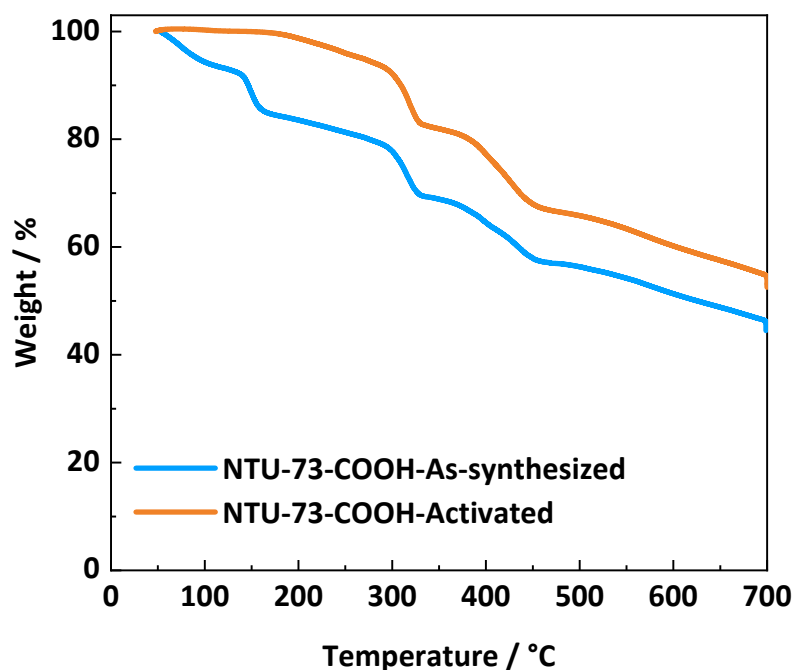


Figure S16. TG curves of as-synthesized and activated NTU-73-COOH.

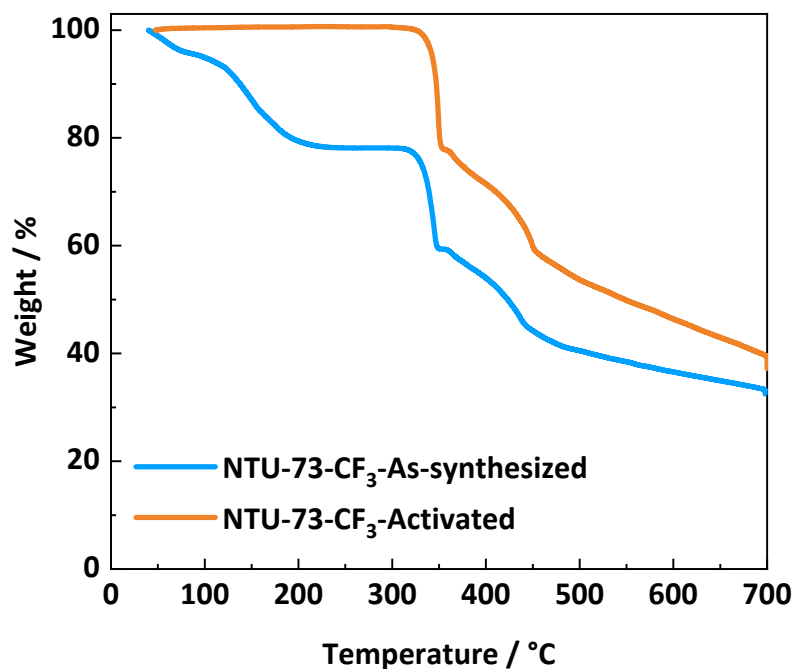


Figure S17. TG curves of as-synthesized and activated NTU-73-CF<sub>3</sub>.

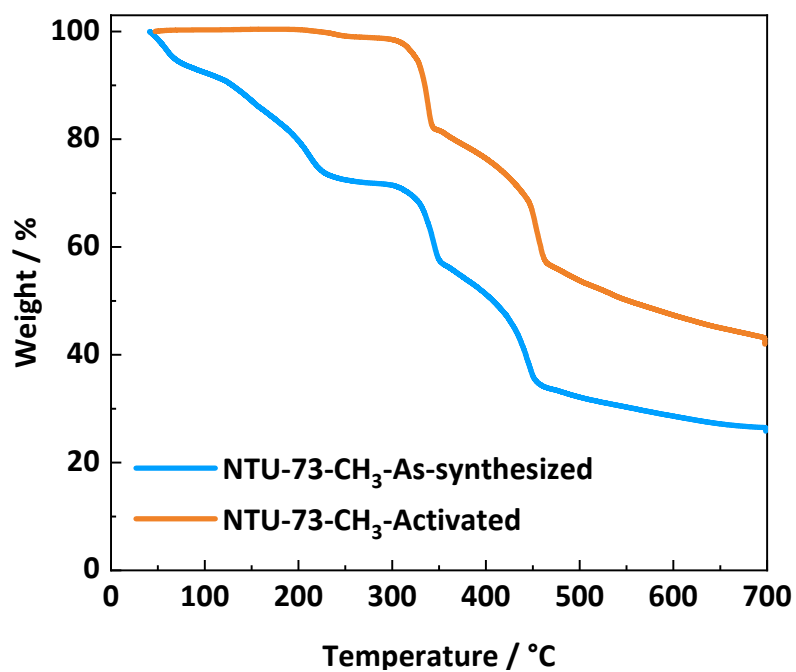


Figure S18. TG curves of as-synthesized and activated NTU-73-CH<sub>3</sub>.

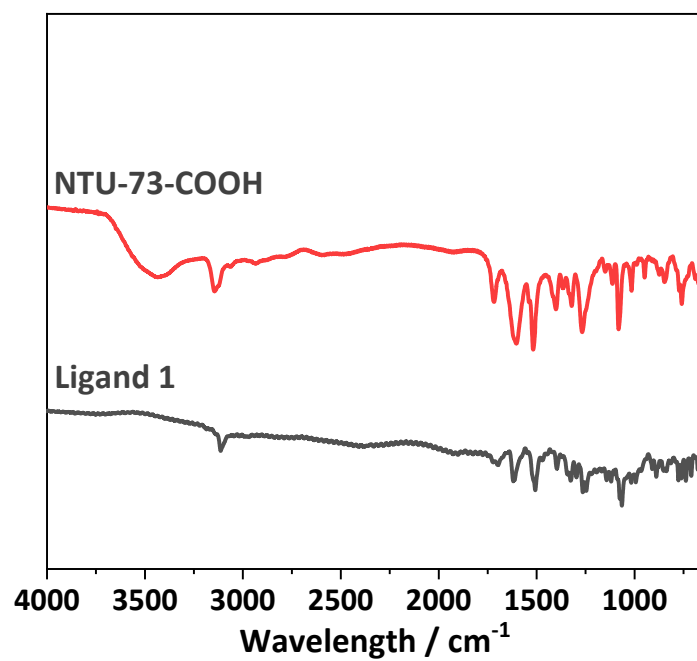


Figure S19. FT-IR spectra of NTU-73-COOH and L1.

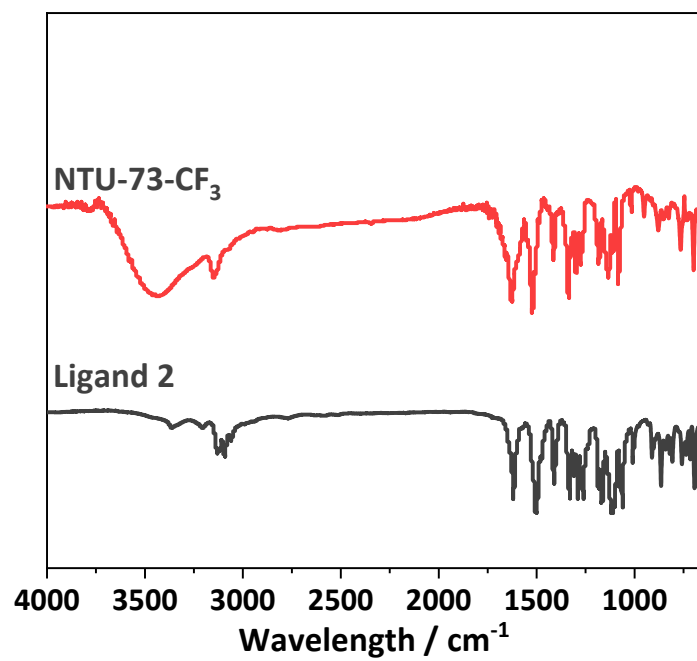


Figure S20. FT-IR spectra of NTU-73-CF<sub>3</sub> and L2.

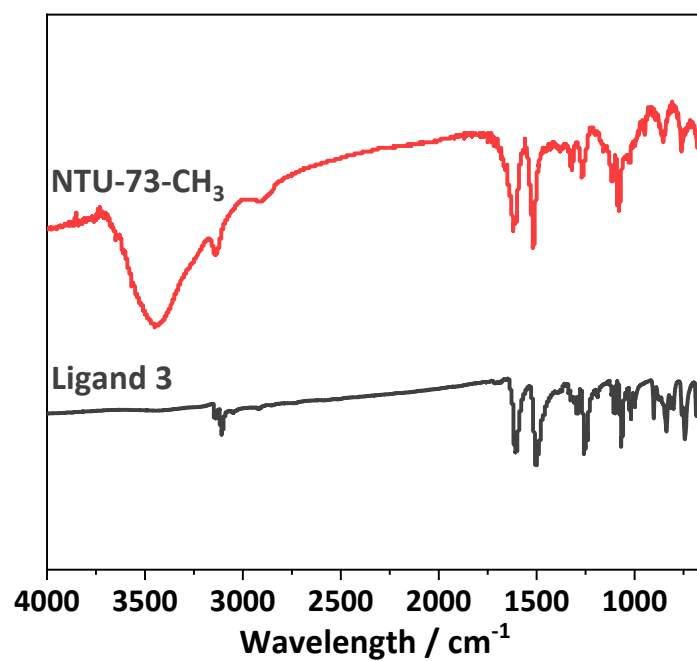


Figure S21. FT-IR spectra of NTU-73-CH<sub>3</sub> and L3.

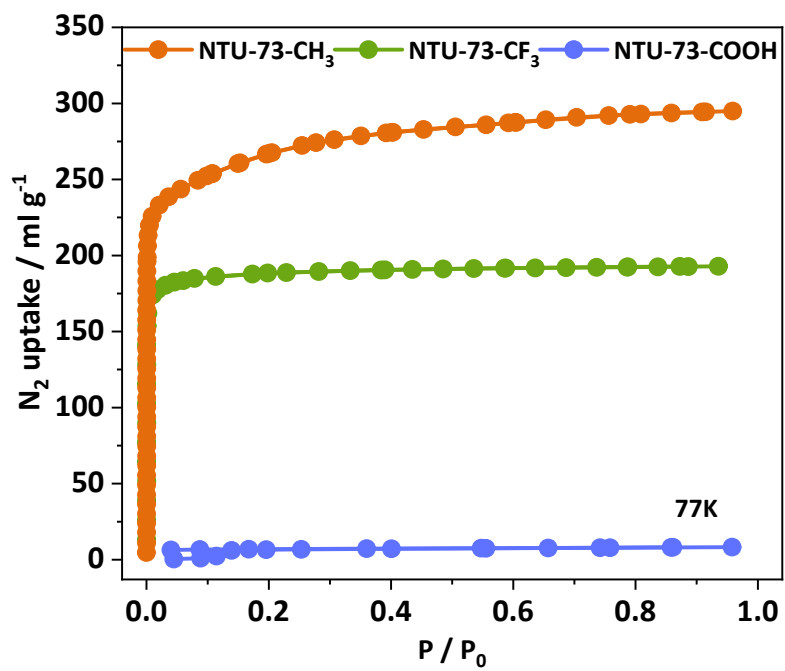


Figure S22. N<sub>2</sub> adsorption isotherms at 77 K.

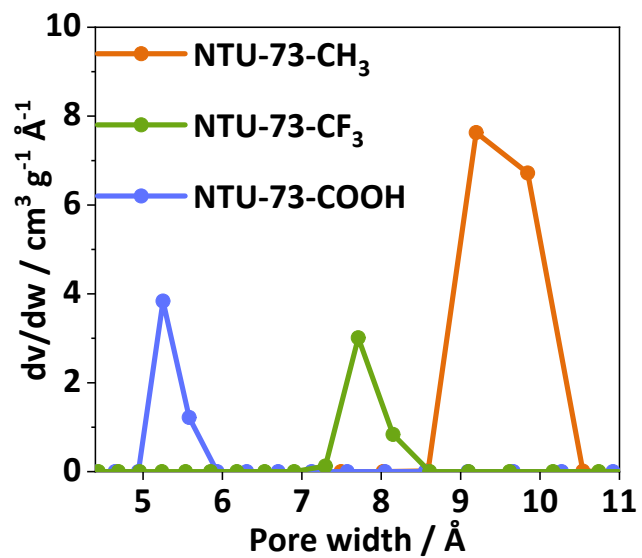


Figure S23. The calculated pore size distributions of the three PCPs.

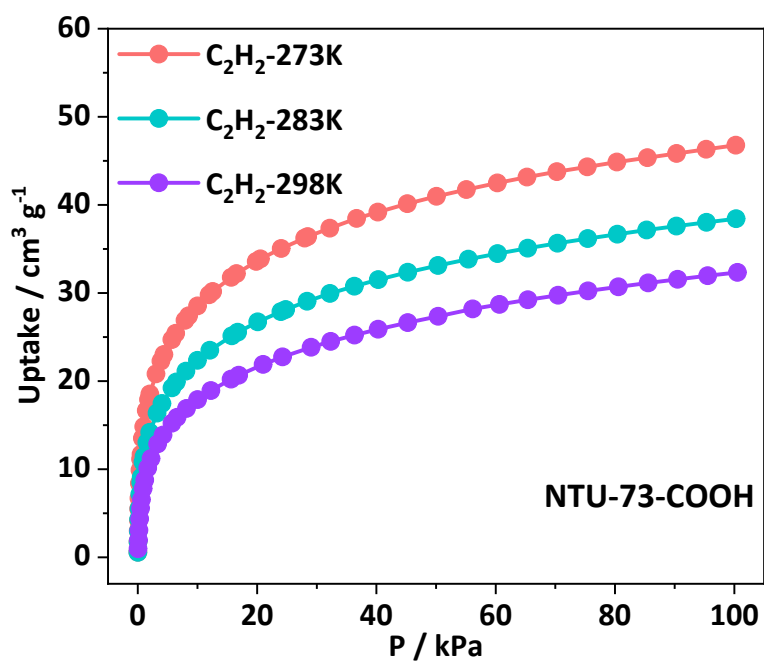


Figure S24. C<sub>2</sub>H<sub>2</sub> adsorption isotherms of NTU-73-COOH.

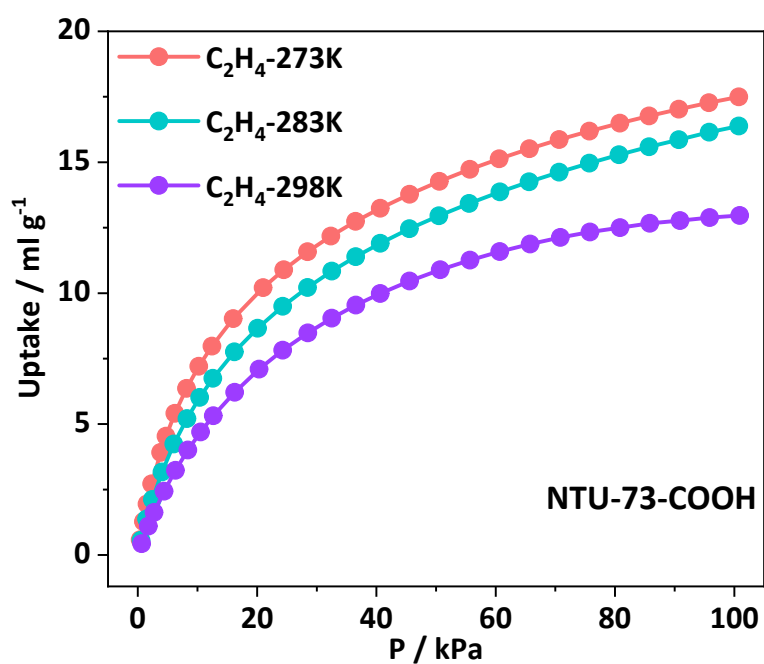


Figure S25.  $C_2H_4$  adsorption isotherms of NTU-73-COOH.

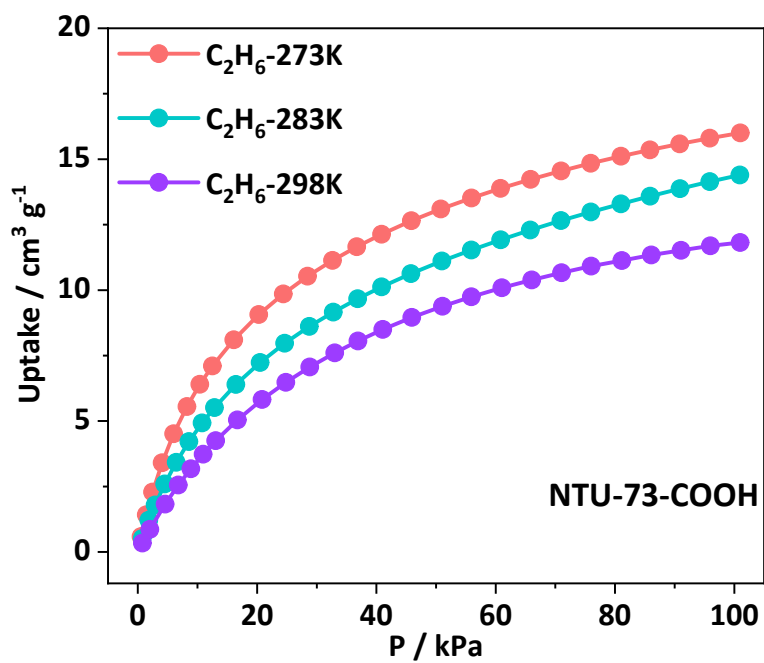


Figure S26.  $C_2H_6$  adsorption isotherms of NTU-73-COOH.

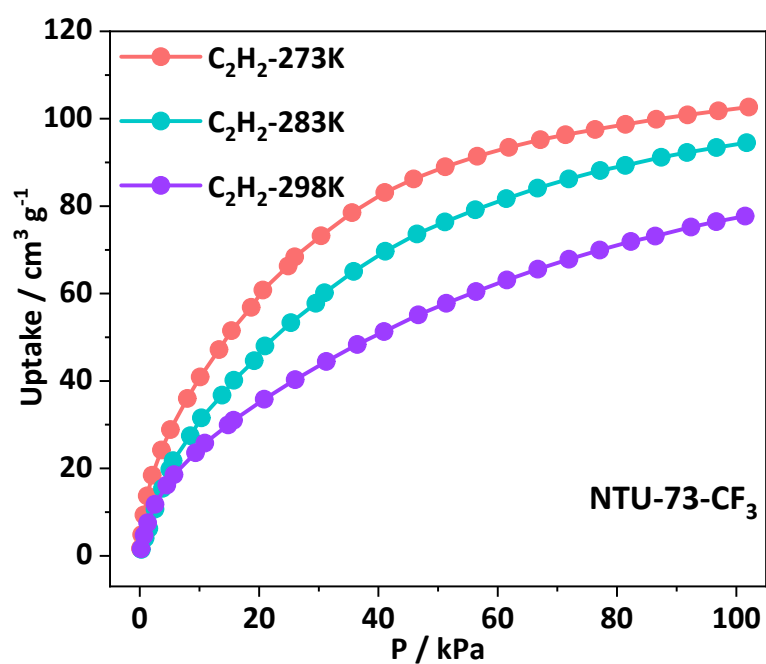


Figure S27.  $C_2H_2$  adsorption isotherms of  $NTU-73-CF_3$ .

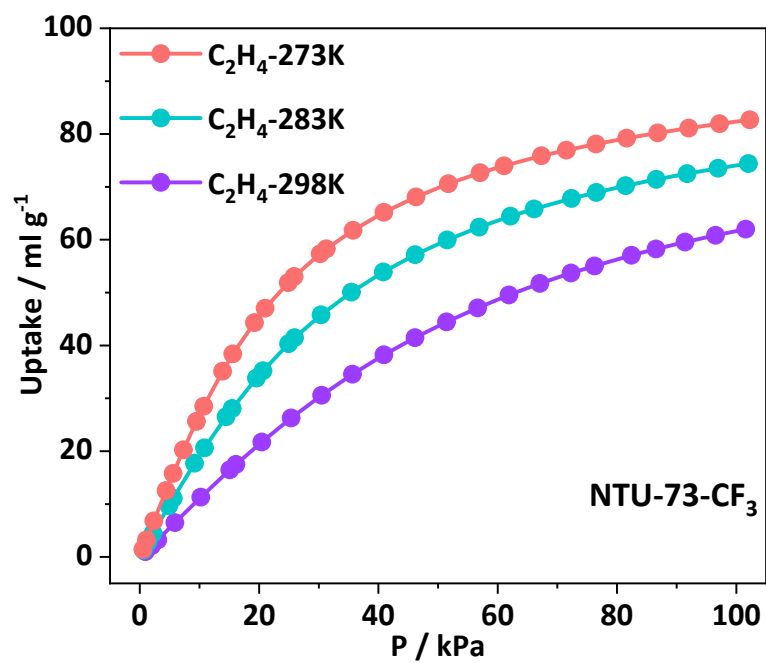


Figure S28.  $C_2H_4$  adsorption isotherms of  $NTU-73-CF_3$ .

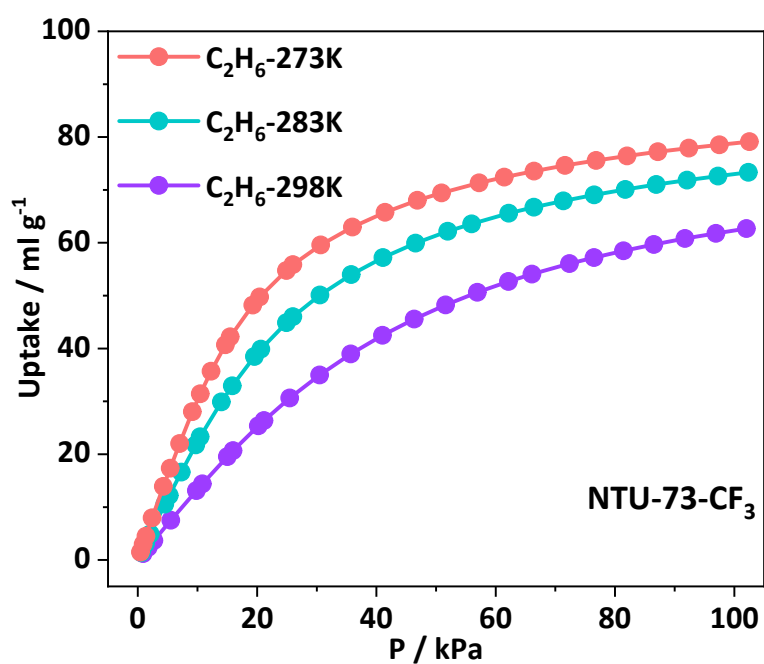


Figure S29.  $C_2H_6$  adsorption isotherms of NTU-73- $CF_3$ .

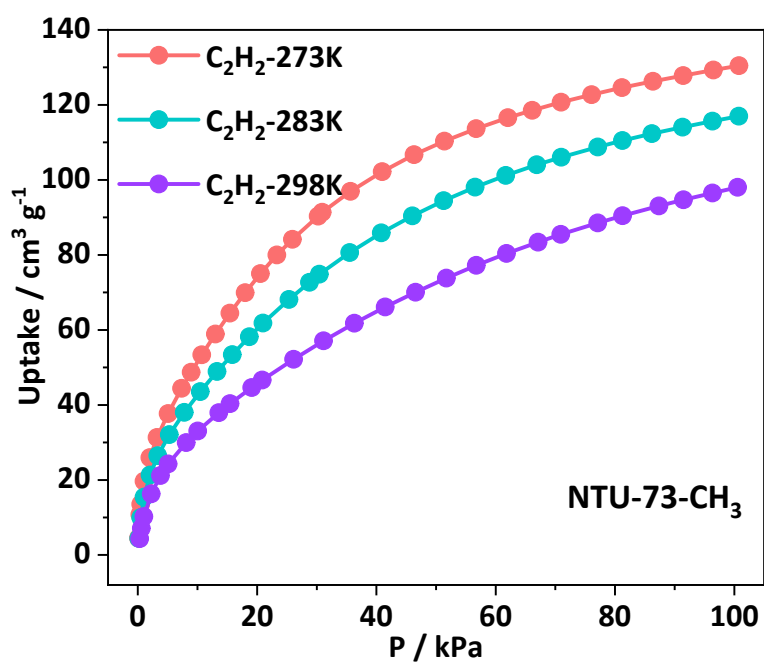


Figure S30.  $C_2H_2$  adsorption isotherms of NTU-73- $CH_3$ .

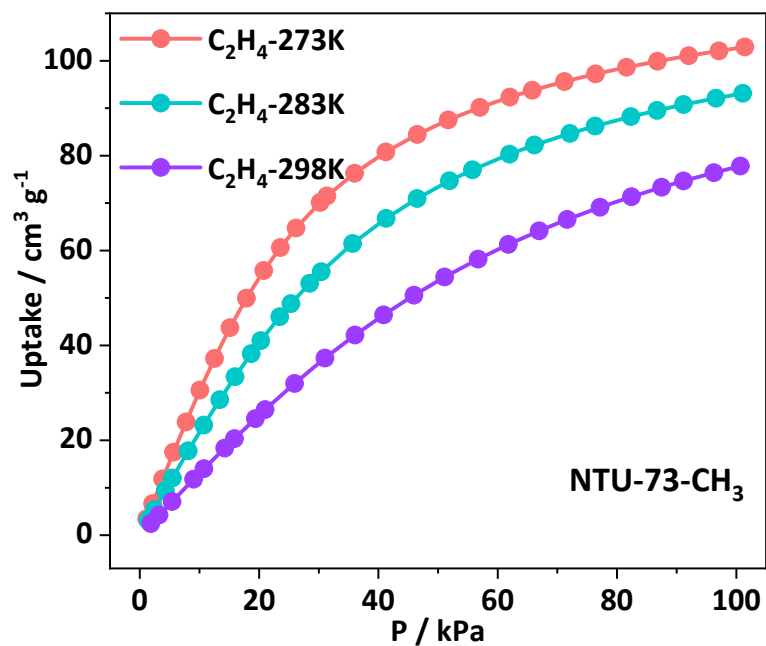


Figure S31. C<sub>2</sub>H<sub>4</sub> adsorption isotherms of NTU-73-CH<sub>3</sub>.

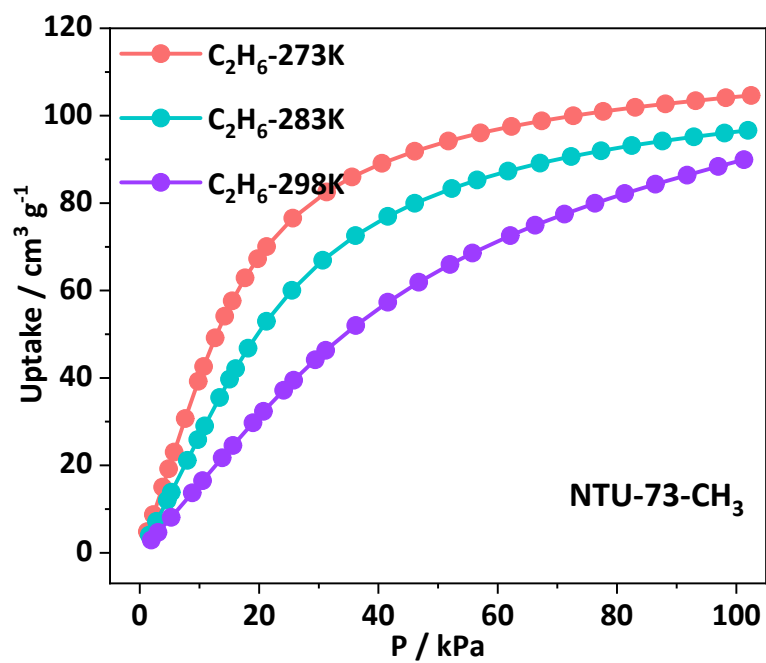


Figure S32. C<sub>2</sub>H<sub>6</sub> adsorption isotherms of NTU-73-CH<sub>3</sub>.

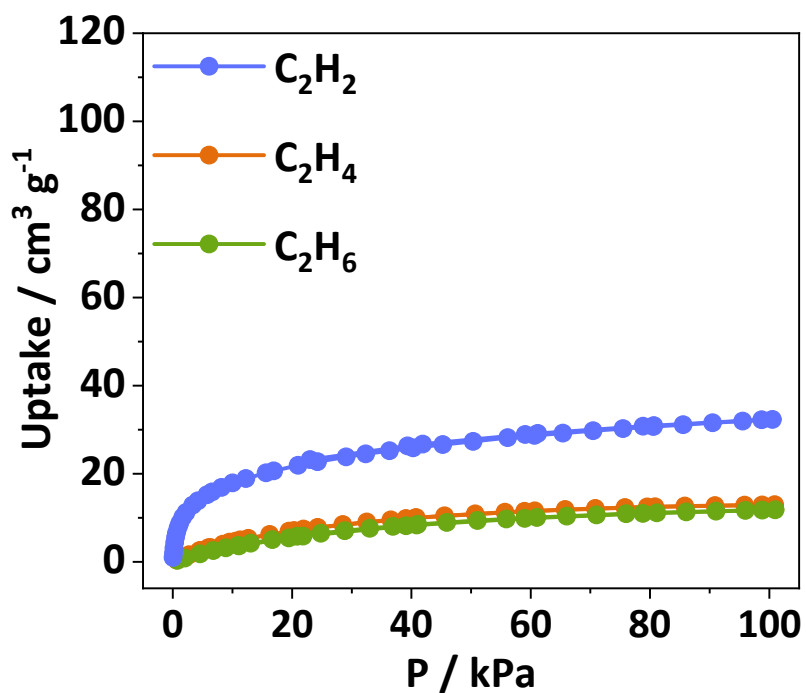


Figure S33. Comparison of the uptakes of C2 hydrocarbons of **NTU-73-COOH** at 298 K, 100 kPa.

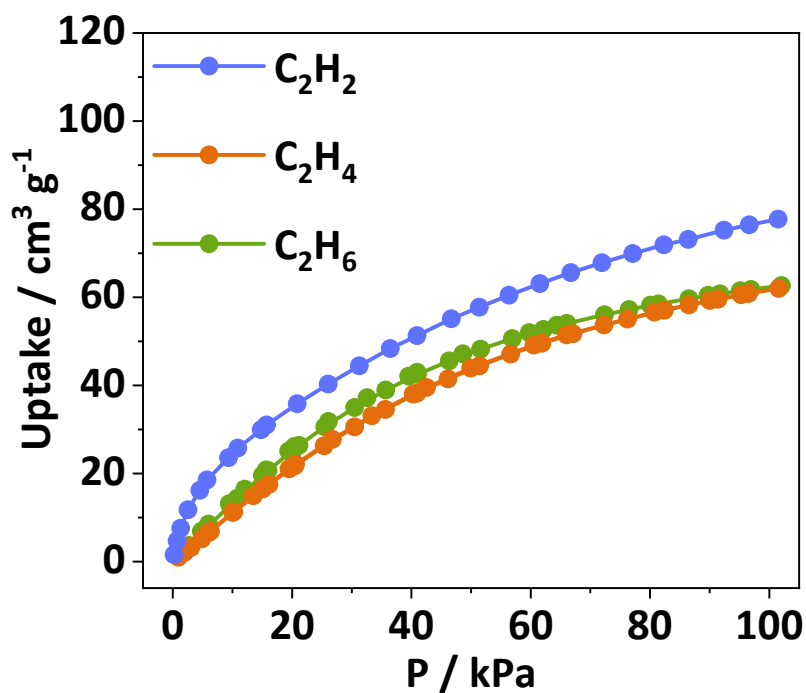


Figure S34. Comparison of the uptakes of C2 hydrocarbons of **NTU-73-CF<sub>3</sub>** at 298 K, 100 kPa.

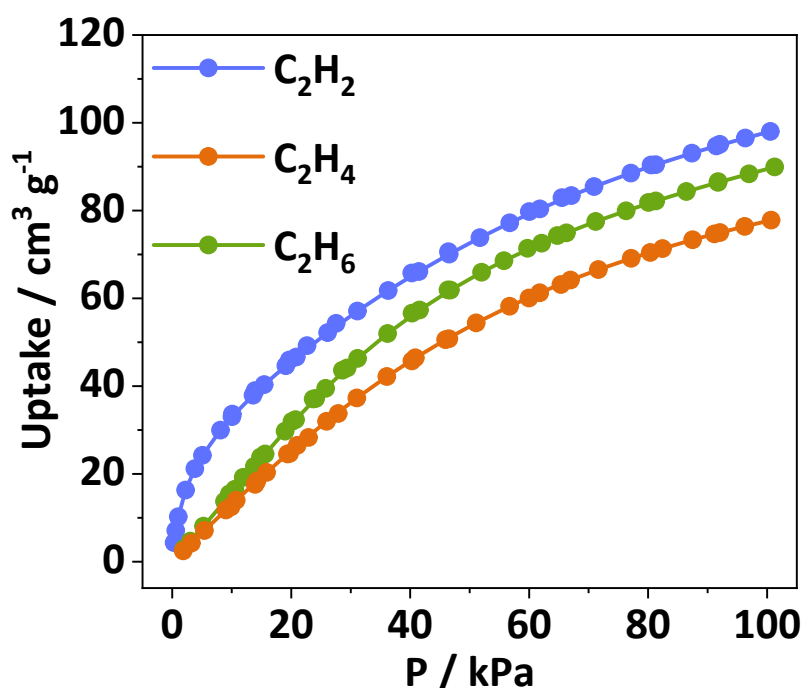


Figure S34. Comparison of the uptakes of C2 hydrocarbons of NTU-73-CH<sub>3</sub> at 298 K, 100 kPa.

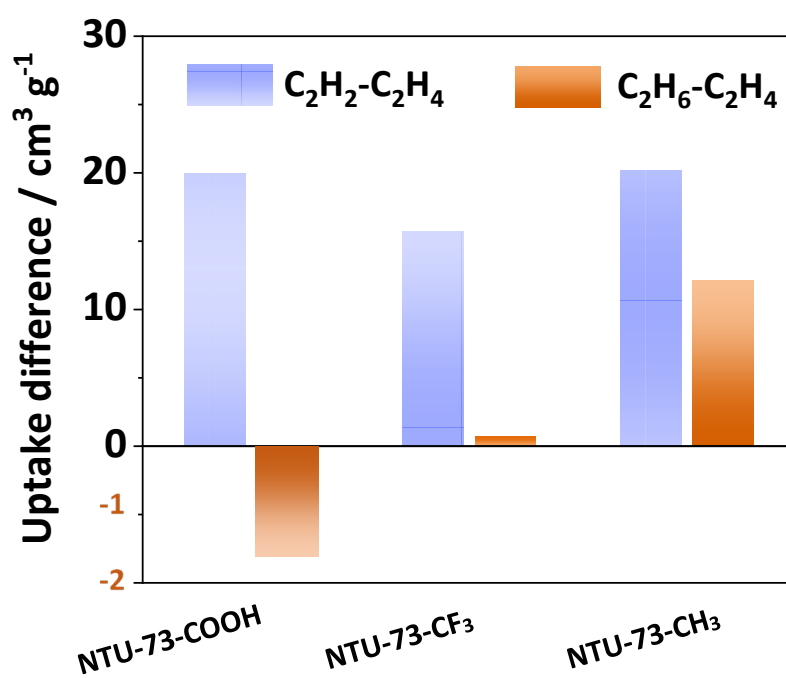


Figure S36. Gas uptake difference of the three samples.

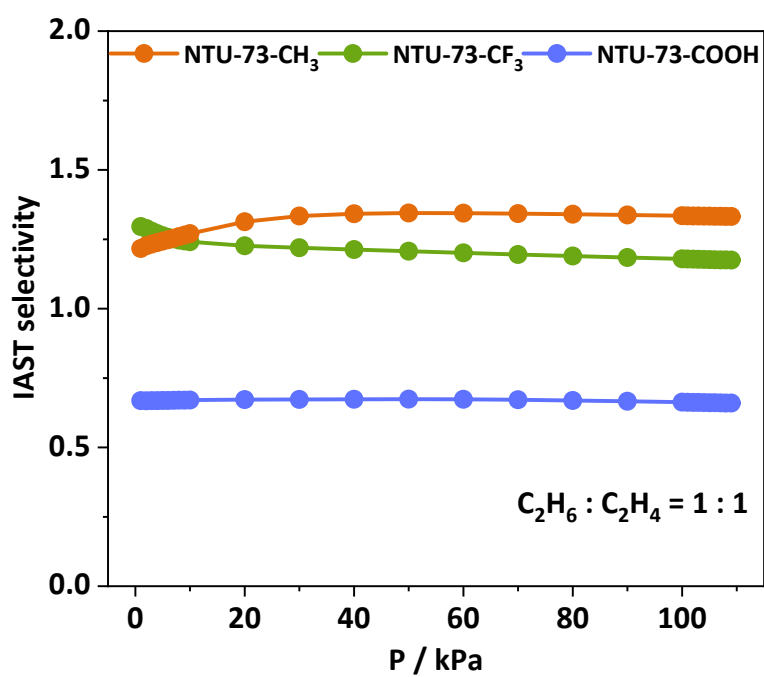


Figure S37. Calculated IAST selectivity of the three PCPs for C<sub>2</sub>H<sub>6</sub>/C<sub>2</sub>H<sub>4</sub> mixture (1/1) at 298 K.

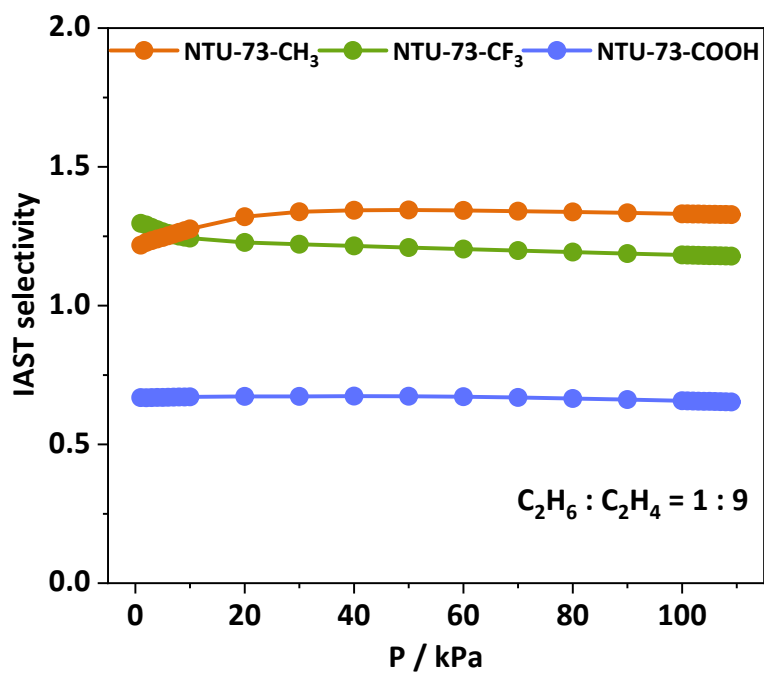


Figure S38. Calculated IAST selectivity of the three PCPs for C<sub>2</sub>H<sub>6</sub>/C<sub>2</sub>H<sub>4</sub> mixture (1/9) at 298 K.

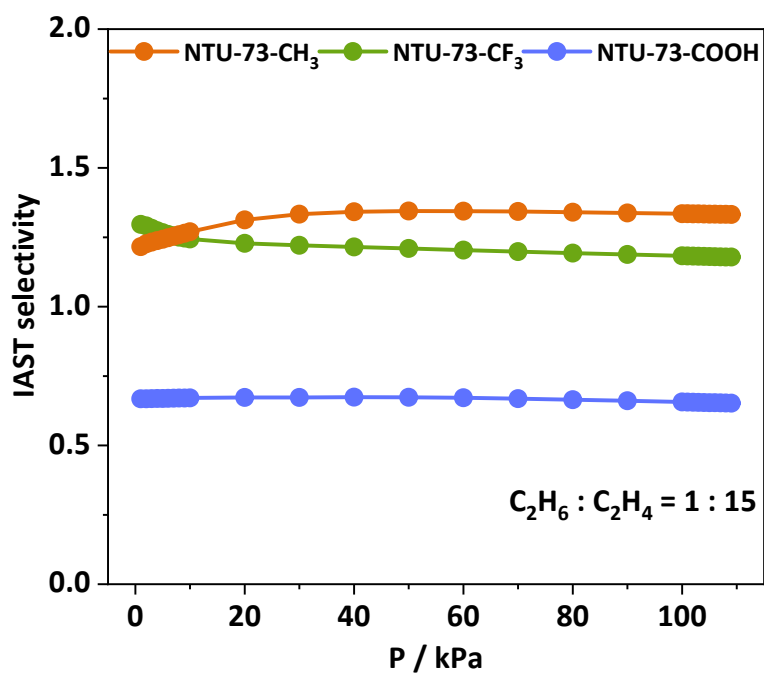


Figure S39. Calculated IAST selectivity of the three PCPs for  $C_2H_6/C_2H_4$  mixture (1/15) at 298 K.

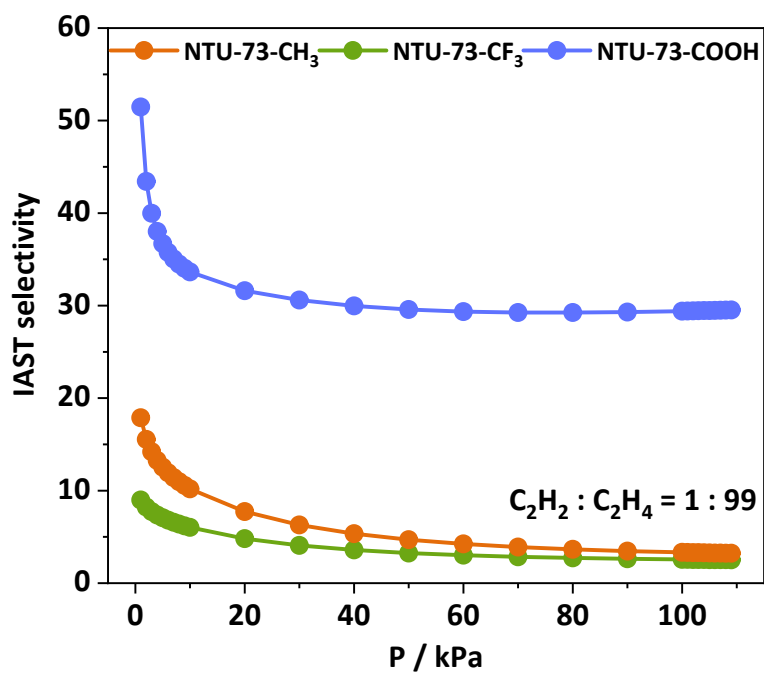


Figure S40. Calculated IAST selectivity of the three PCPs for  $C_2H_2/C_2H_4$  mixture (1/99) at 298 K.

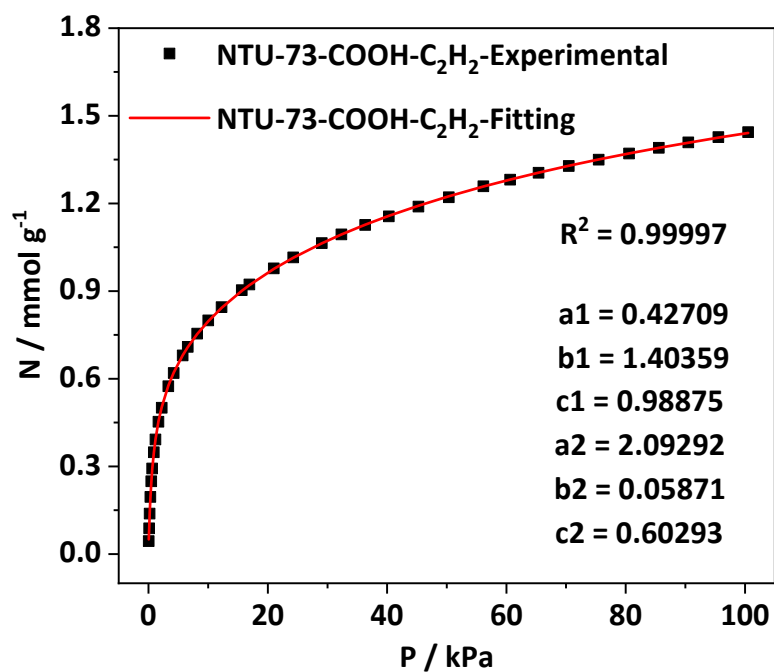


Figure S41. Curves fitting of  $C_2H_2$  adsorption isotherm for NTU-73-COOH at 298 K.

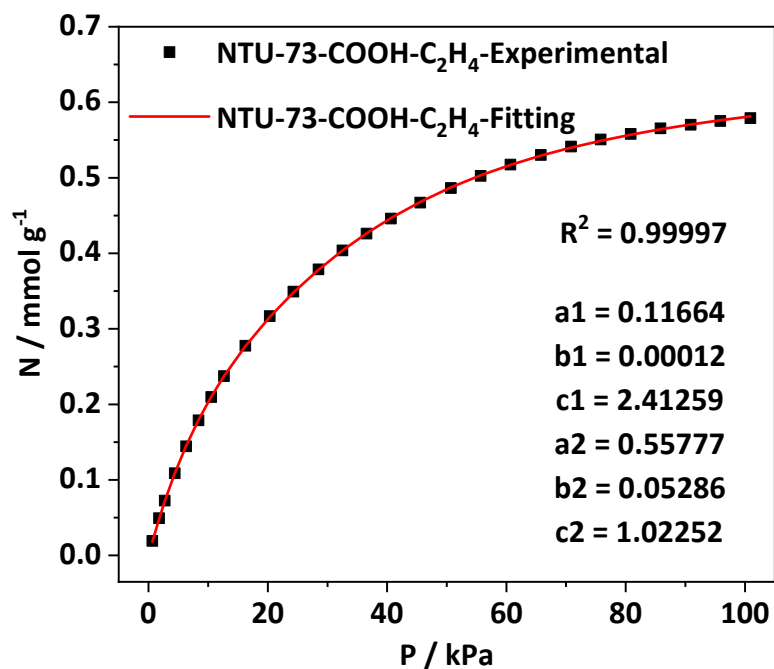


Figure S42. Curves fitting of  $C_2H_4$  adsorption isotherm for NTU-73-COOH at 298 K.

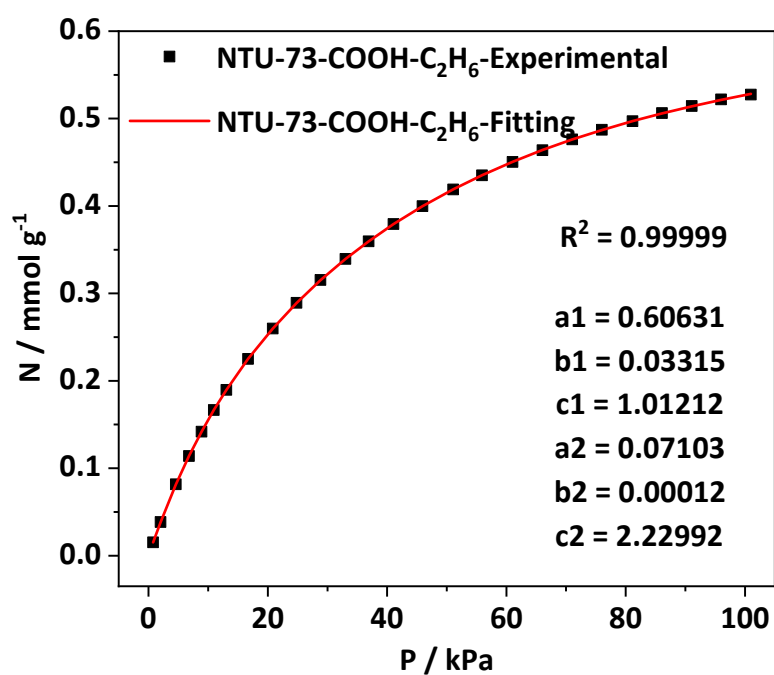


Figure S43. Curves fitting of C<sub>2</sub>H<sub>6</sub> adsorption isotherm for NTU-73-COOH at 298 K.

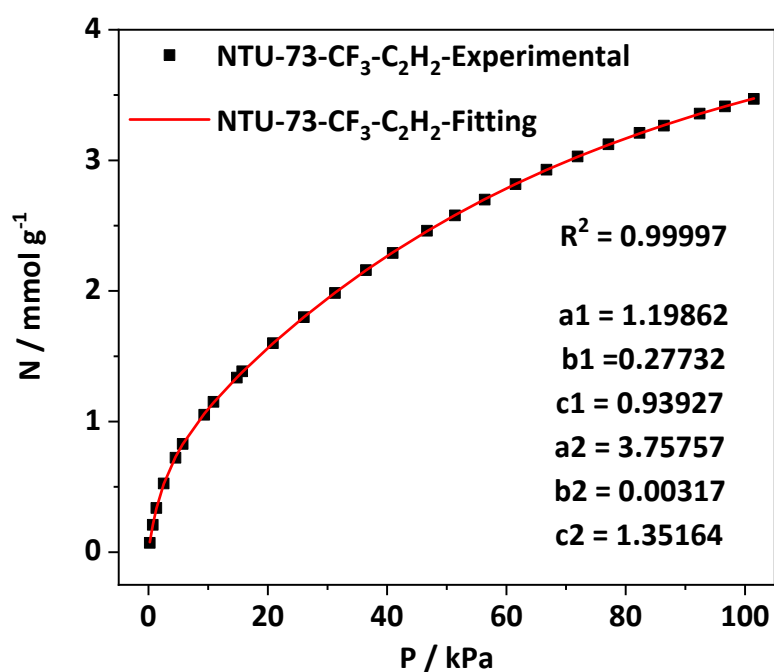


Figure S44. Curves fitting of C<sub>2</sub>H<sub>2</sub> adsorption isotherm for NTU-73-CF<sub>3</sub> at 298 K.

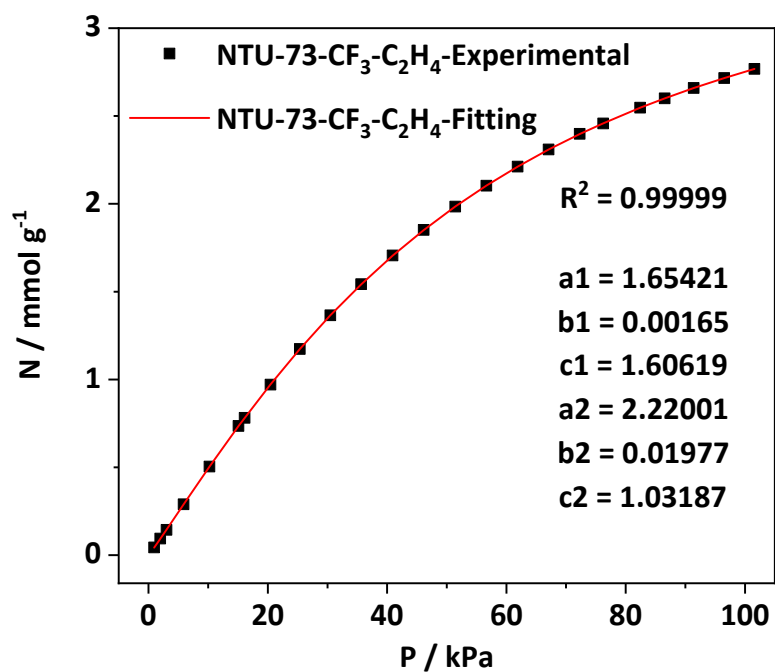


Figure S45. Curves fitting of C<sub>2</sub>H<sub>4</sub> adsorption isotherm for NTU-73-CF<sub>3</sub> at 298 K.

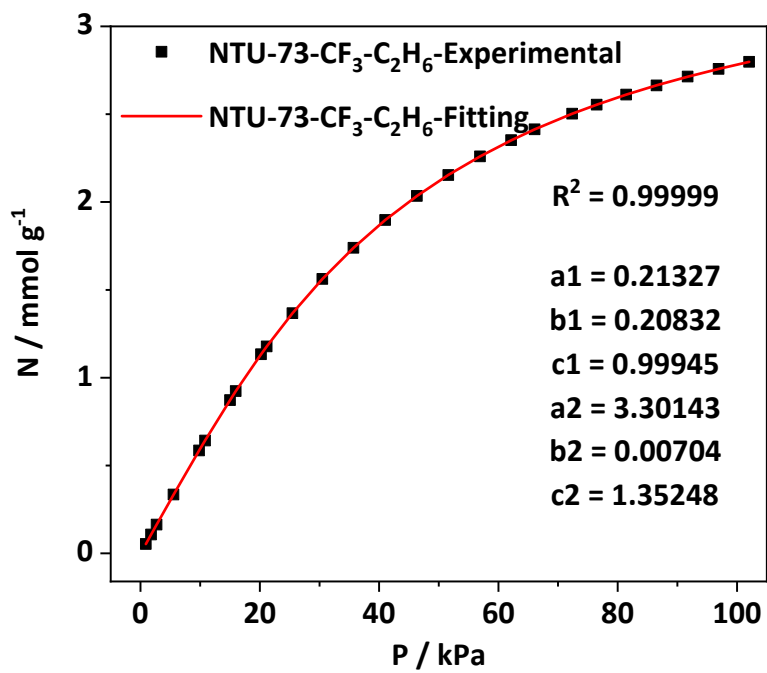


Figure S46. Curves fitting of C<sub>2</sub>H<sub>6</sub> adsorption isotherm for NTU-73-CF<sub>3</sub> at 298 K.

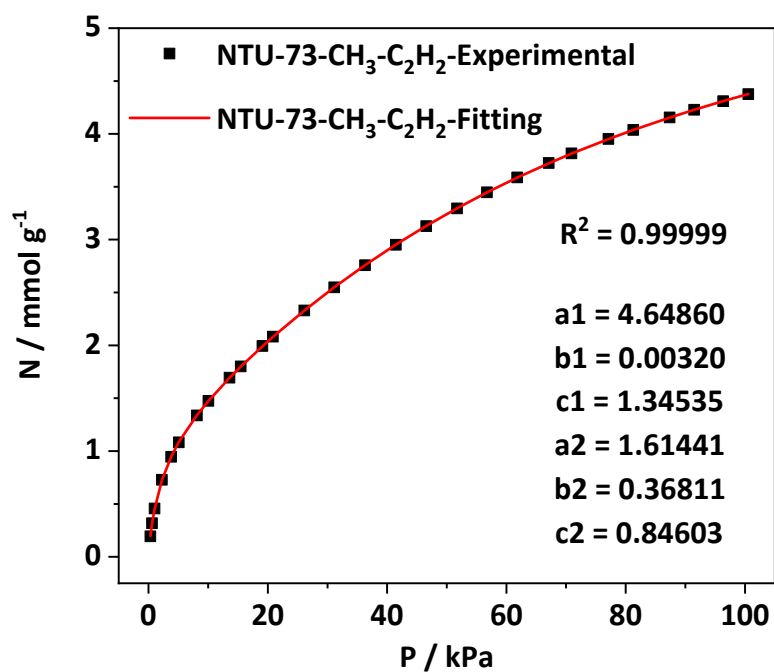


Figure S47. Curves fitting of C<sub>2</sub>H<sub>2</sub> adsorption isotherm for NTU-73-CH<sub>3</sub> at 298 K.

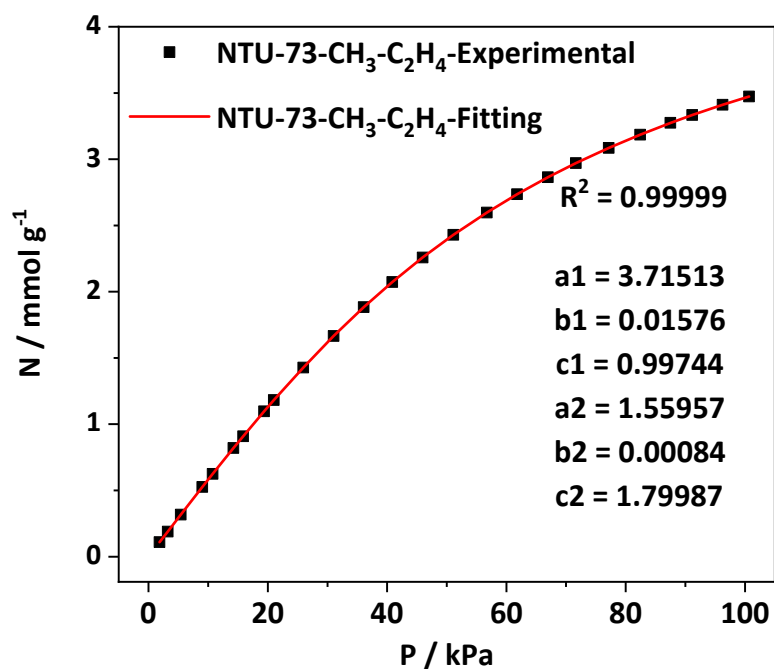


Figure S48. Curves fitting of C<sub>2</sub>H<sub>4</sub> adsorption isotherm for NTU-73-CH<sub>3</sub> at 298 K.

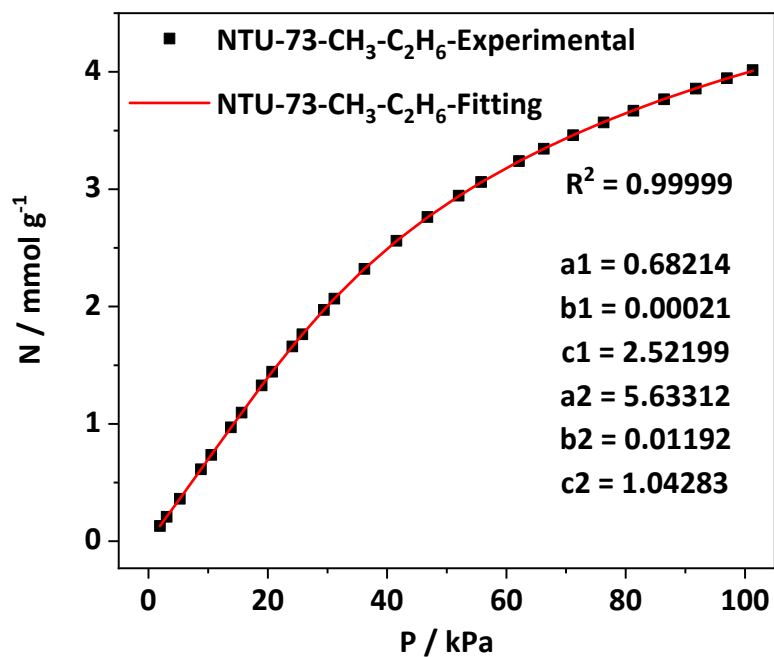


Figure S49. Curves fitting of C<sub>2</sub>H<sub>6</sub> adsorption isotherm for NTU-73-CH<sub>3</sub> at 298 K.

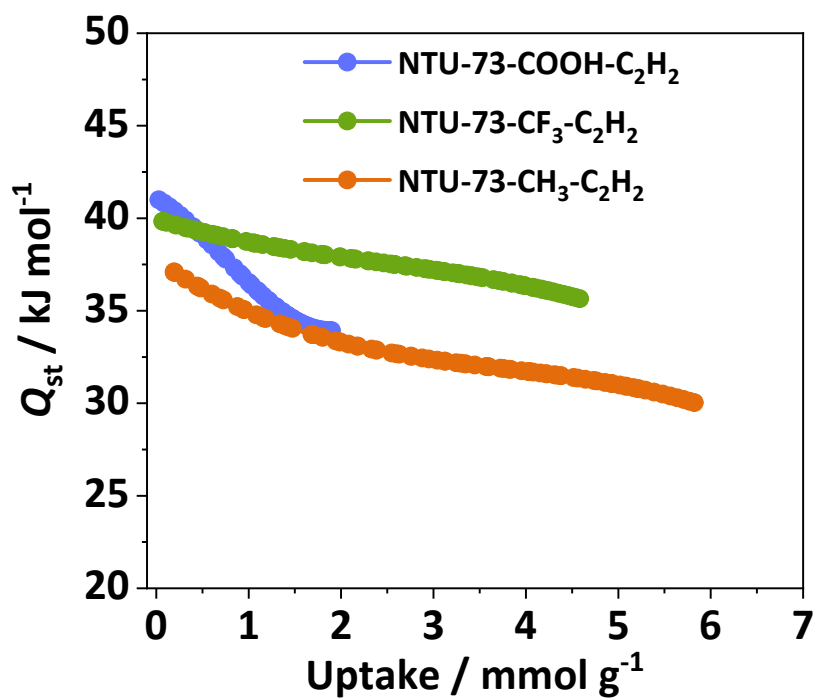
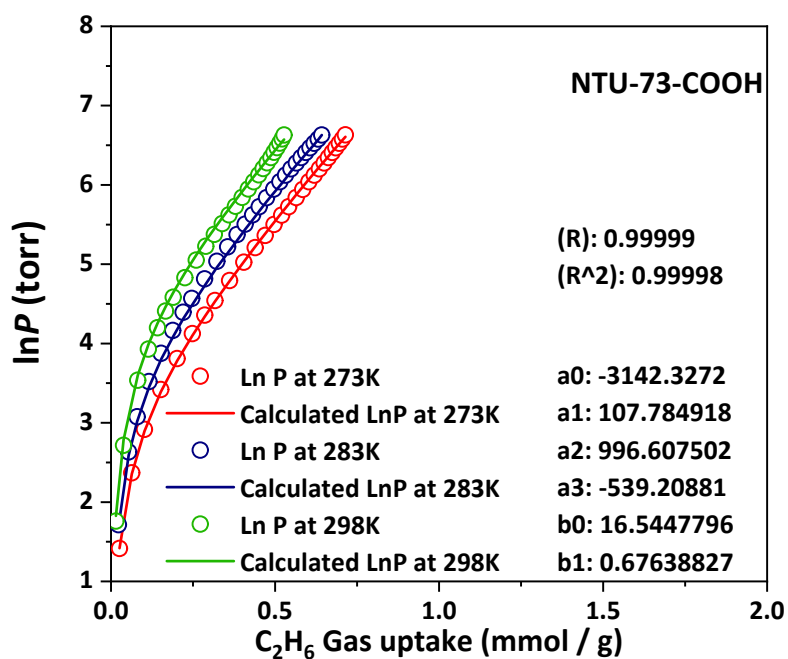
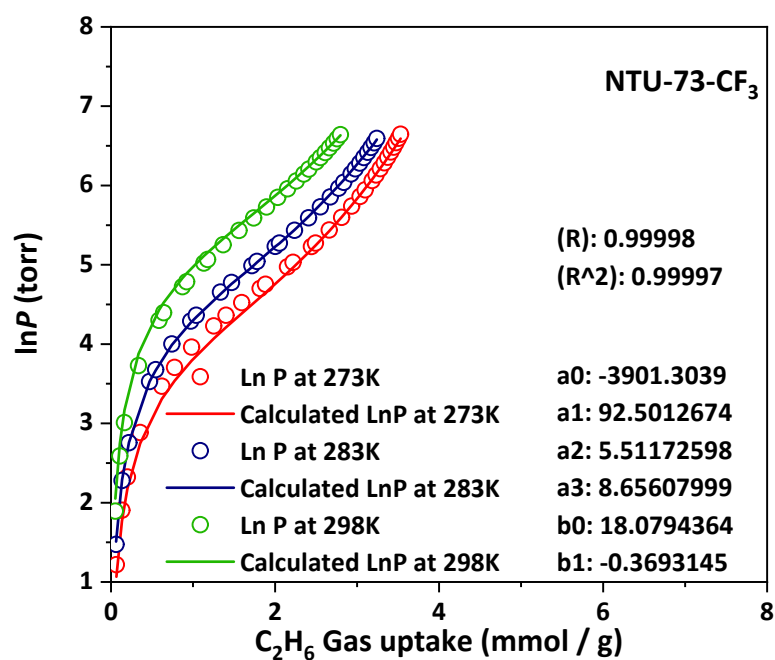


Figure S50. C<sub>2</sub>H<sub>2</sub> isosteric heats of the three PCPs.



**Figure S51.** The calculated virial equation isotherms fit to the experimental C<sub>2</sub>H<sub>6</sub> data of **NTU-73-COOH**.



**Figure S52.** The calculated virial equation isotherms fit to the experimental C<sub>2</sub>H<sub>6</sub> data of **NTU-73-CF<sub>3</sub>**.

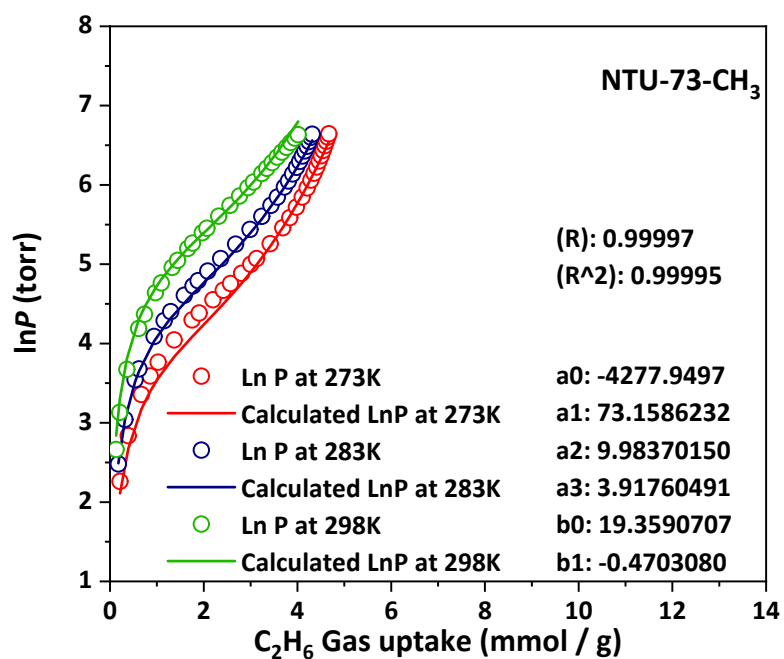


**Figure S53.** The calculated virial equation isotherms fit to the experimental C<sub>2</sub>H<sub>6</sub> data of **NTU-73-CH<sub>3</sub>**.

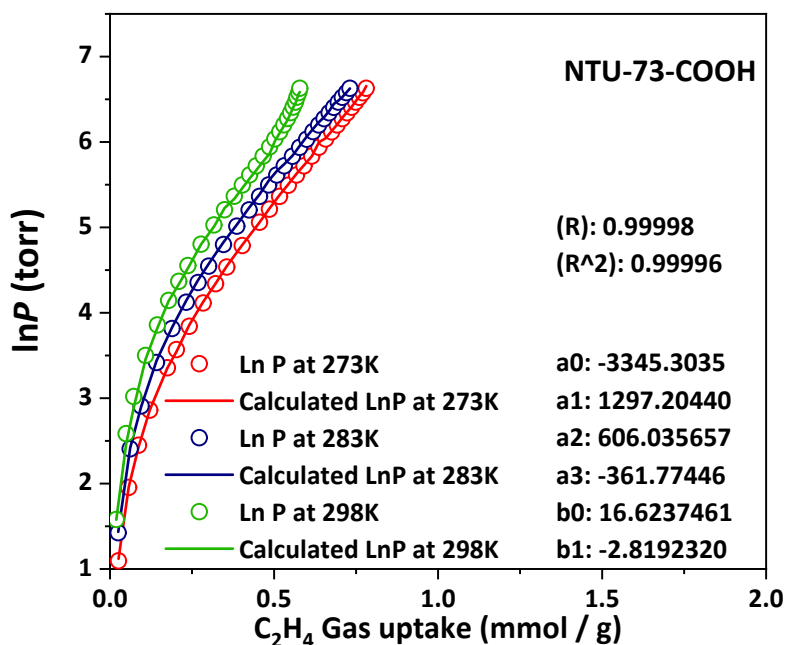


**Figure S54.** The calculated virial equation isotherms fit to the experimental C<sub>2</sub>H<sub>4</sub> data of **NTU-73-COOH**.

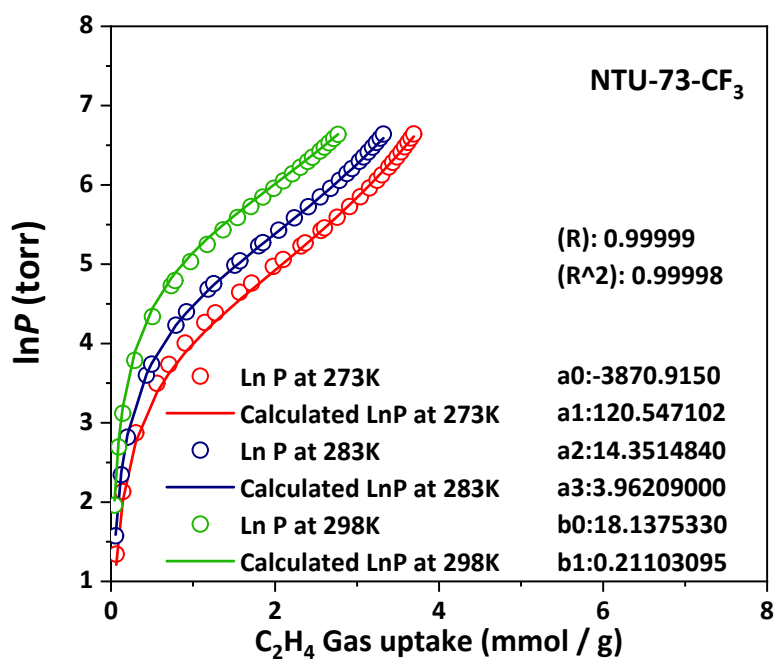


Figure S55. The calculated virial equation isotherms fit to the experimental C<sub>2</sub>H<sub>4</sub> data of NTU-73-CF<sub>3</sub>.

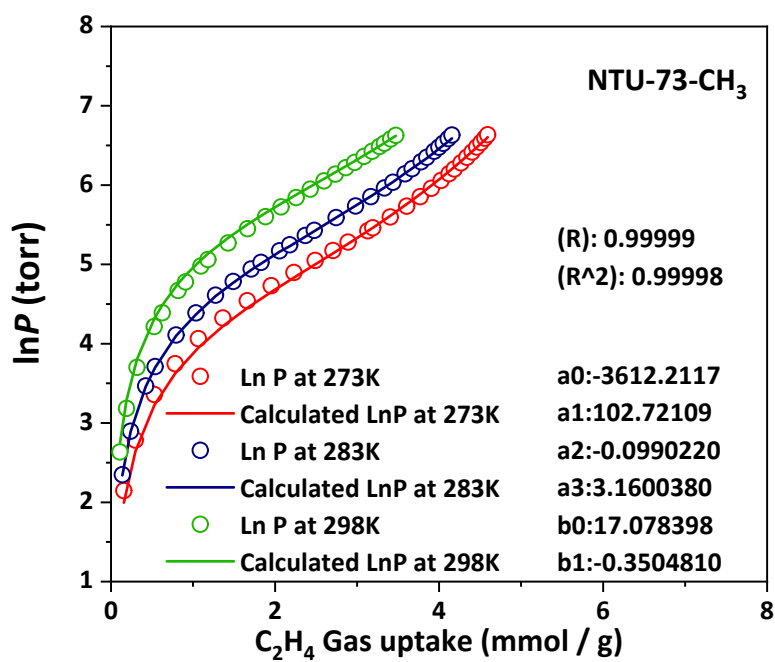
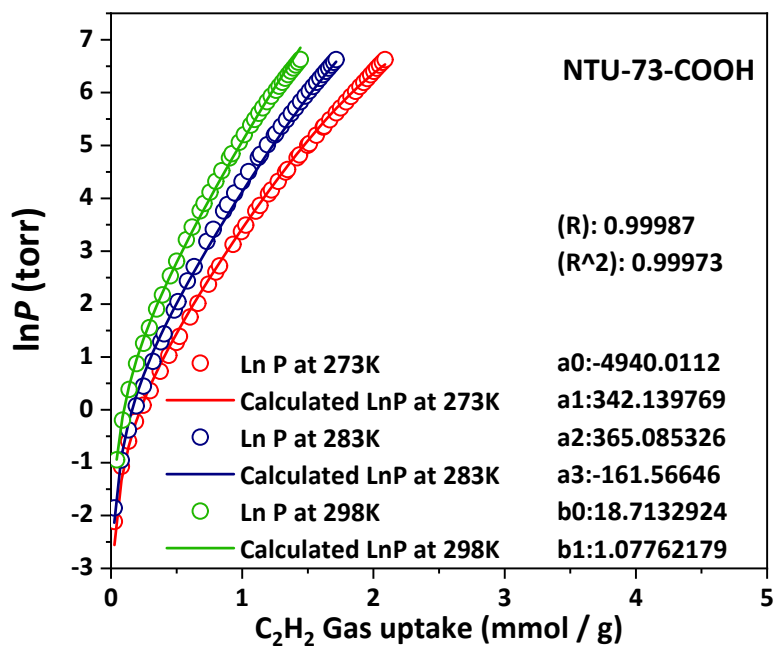
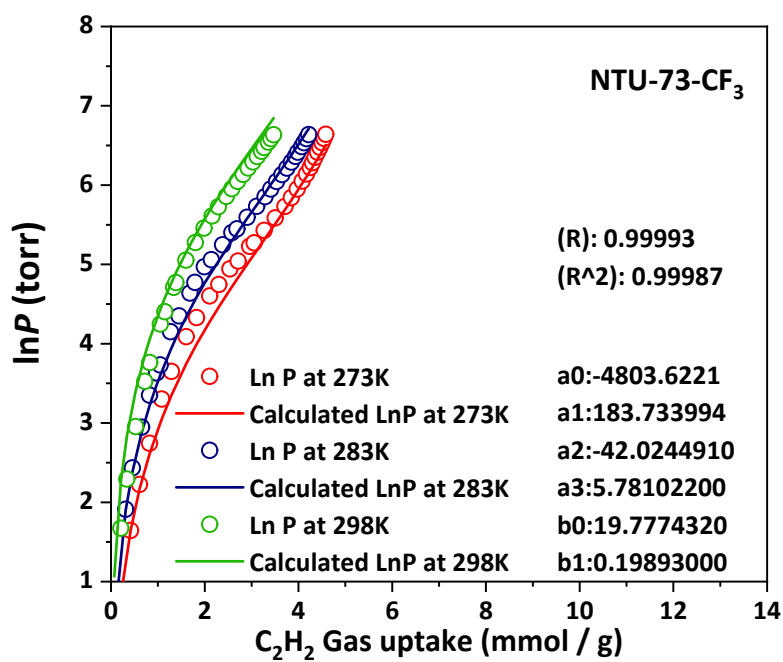


Figure S56. The calculated virial equation isotherms fit to the experimental C<sub>2</sub>H<sub>4</sub> data of NTU-73-CH<sub>3</sub>.



**Figure S57.** The calculated virial equation isotherms fit to the experimental C<sub>2</sub>H<sub>2</sub> data of **NTU-73-COOH**.



**Figure S58.** The calculated virial equation isotherms fit to the experimental C<sub>2</sub>H<sub>2</sub> data of **NTU-73-CF<sub>3</sub>**.

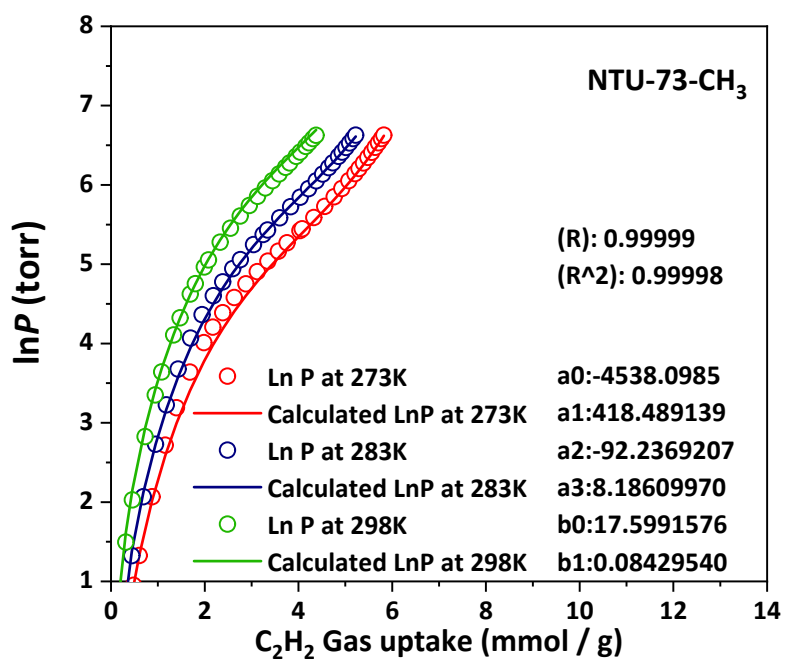


Figure S59. The calculated virial equation isotherms fit to the experimental  $C_2H_2$  data of NTU-73- $CH_3$ .

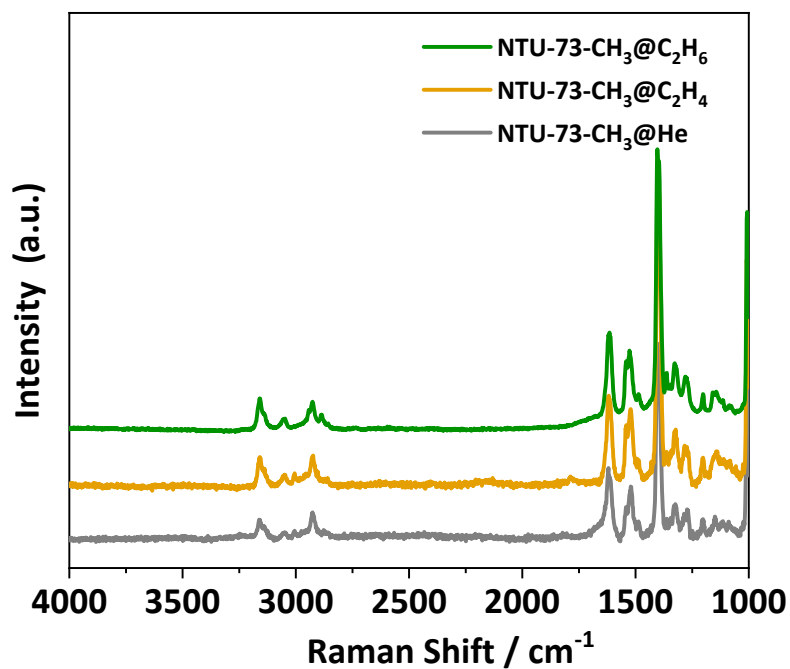


Figure S60. Raman spectra of gas-loaded NTU-73- $CH_3$  in the range of 1000 to 4000  $cm^{-1}$ .

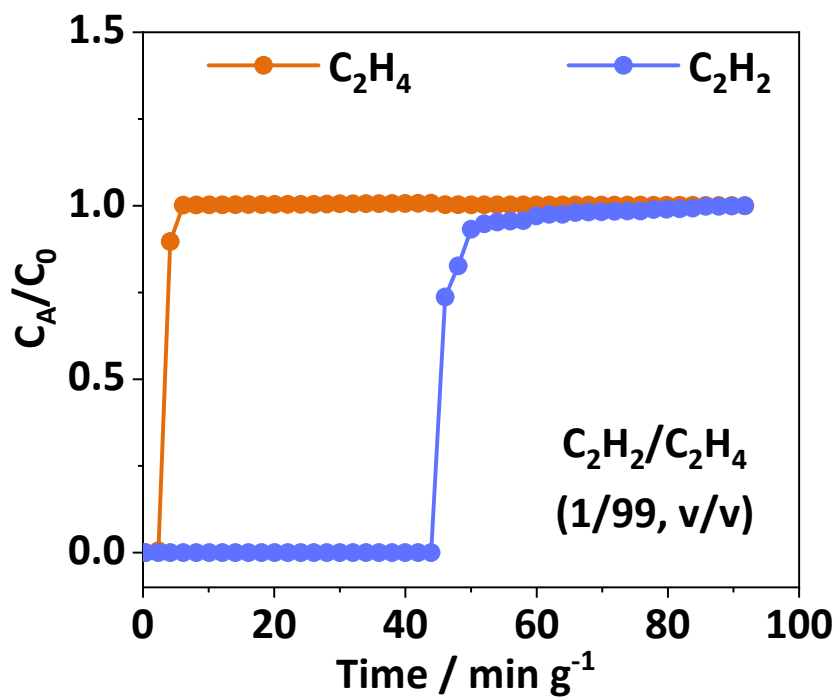


Figure S61. Experimental breakthrough curves of NTU-73-COOH for  $C_2H_2/C_2H_4$  (1/99, v/v, 2 mL  $\text{min}^{-1}$ ) mixtures at 298 K.

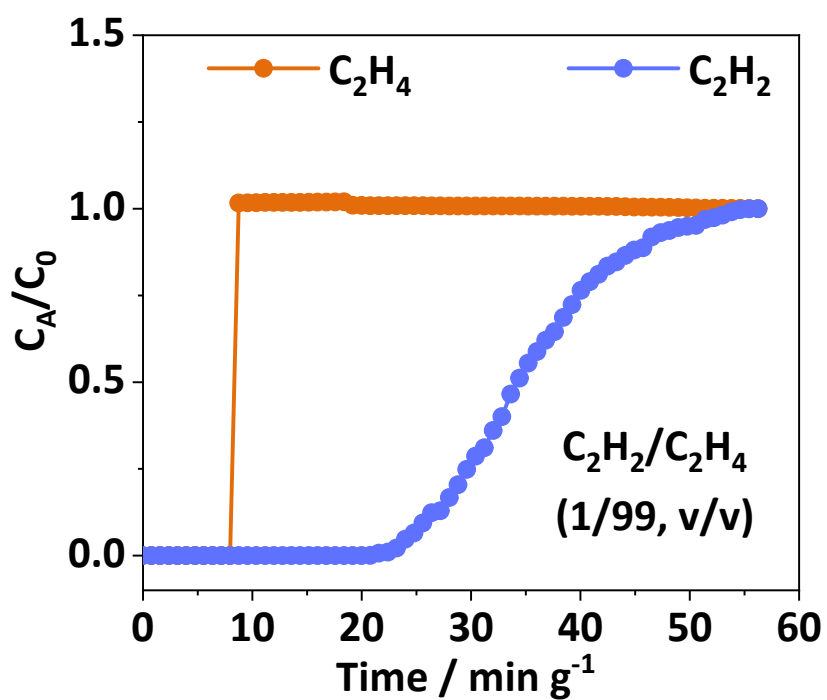


Figure S62. Experimental breakthrough curves of NTU-73-CF<sub>3</sub> for  $C_2H_2/C_2H_4$  (1/99, v/v, 2 mL  $\text{min}^{-1}$ ) mixtures at 298 K.

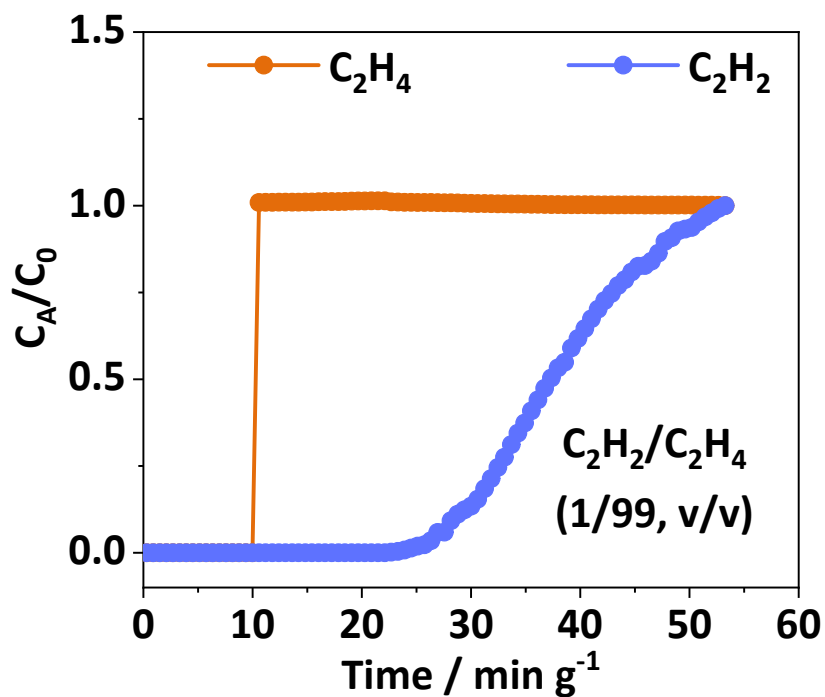


Figure S63. Experimental breakthrough curves of NTU-73-CH<sub>3</sub> for C<sub>2</sub>H<sub>2</sub>/C<sub>2</sub>H<sub>4</sub> (1/99, v/v, 2 mL min<sup>-1</sup>) mixtures at 298 K.

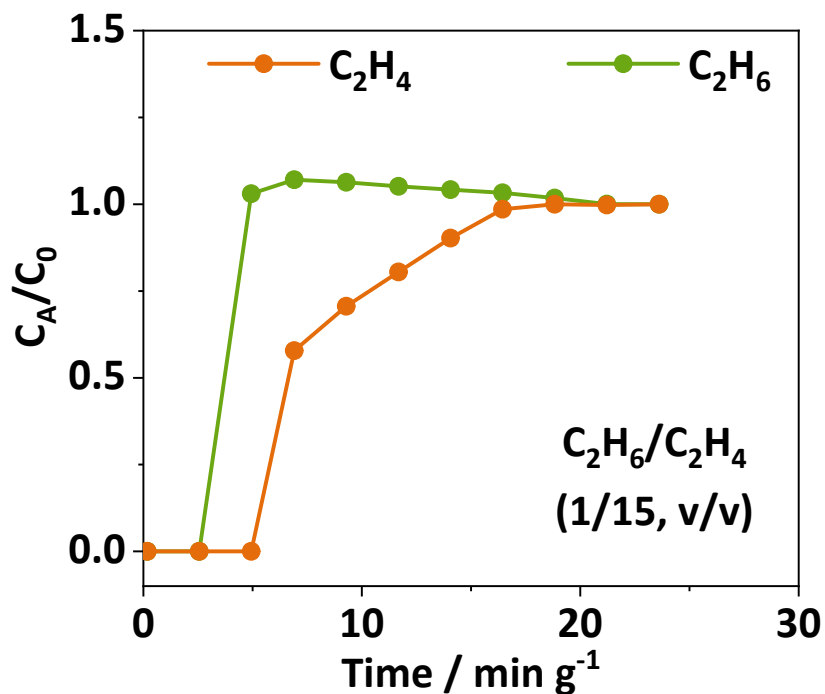


Figure S64. Experimental breakthrough curves of NTU-73-COOH for C<sub>2</sub>H<sub>6</sub>/C<sub>2</sub>H<sub>4</sub> (1/15, v/v, 2 mL min<sup>-1</sup>) mixtures at 298 K.

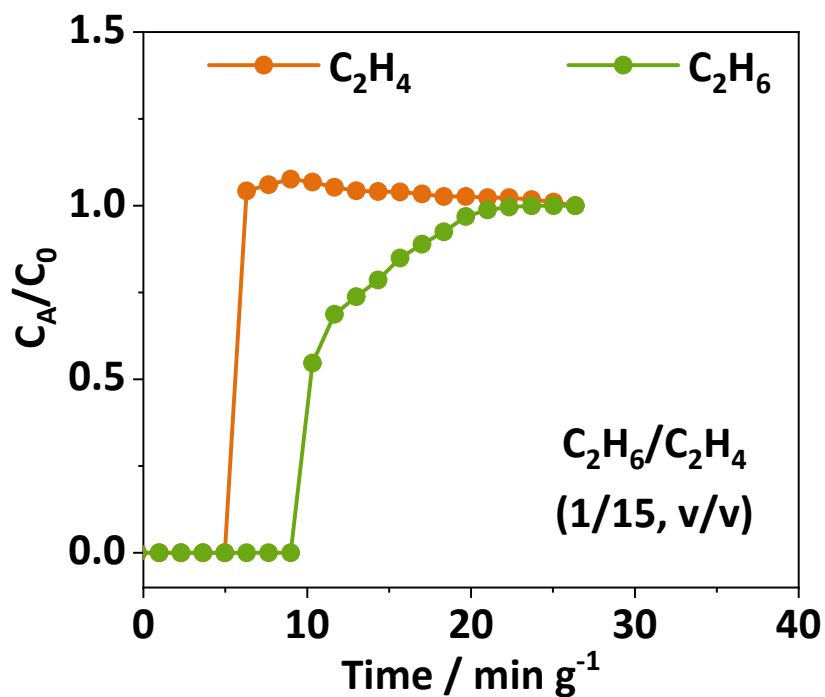


Figure S65. Experimental breakthrough curves of NTU-73-CF<sub>3</sub> for C<sub>2</sub>H<sub>6</sub>/C<sub>2</sub>H<sub>4</sub> (1/15, v/v, 2 mL min<sup>-1</sup>) mixtures at 298 K.

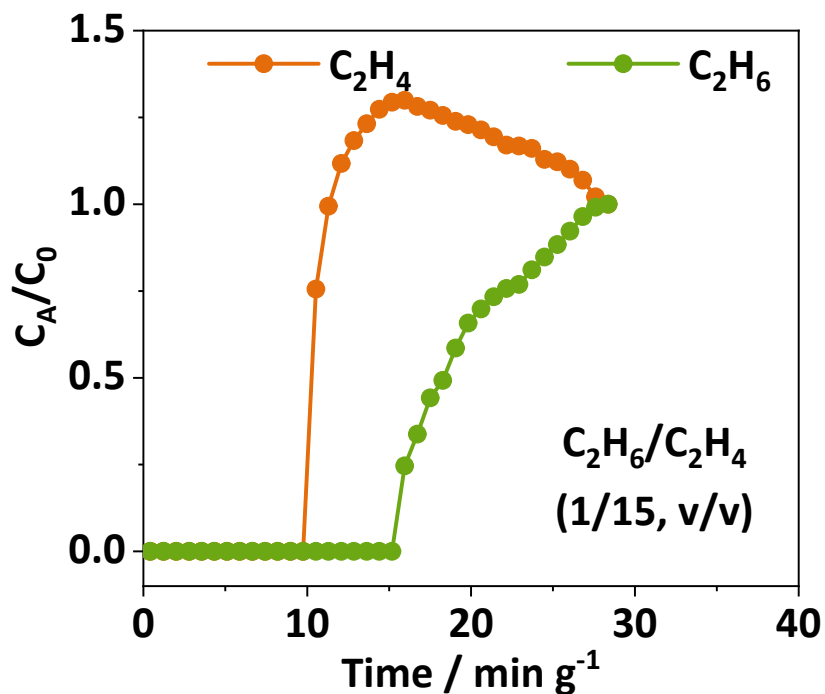


Figure S66. Experimental breakthrough curves of NTU-73-CH<sub>3</sub> for C<sub>2</sub>H<sub>6</sub>/C<sub>2</sub>H<sub>4</sub> (1/15, v/v, 2 mL min<sup>-1</sup>) mixtures at 298 K.

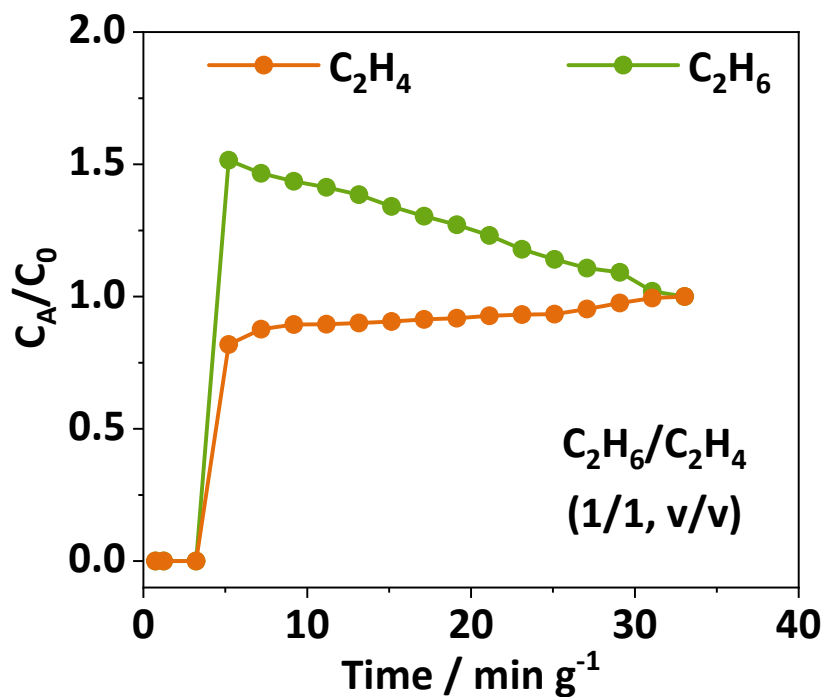


Figure S67. Experimental breakthrough curves of NTU-73-COOH for  $C_2H_6/C_2H_4$  (1/1, v/v, 2 mL  $\text{min}^{-1}$ ) mixtures at 298 K.

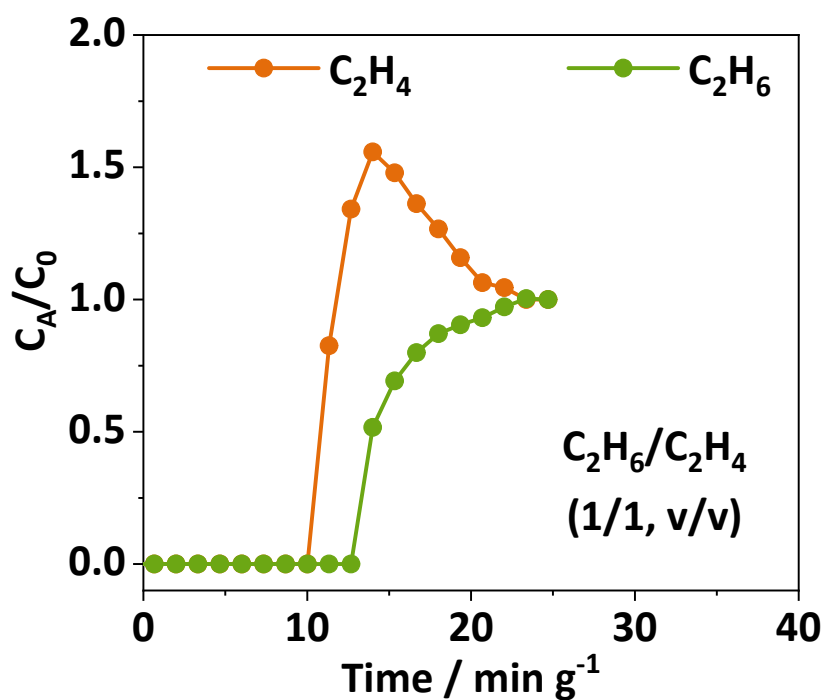


Figure S68. Experimental breakthrough curves of NTU-73-CF<sub>3</sub> for  $C_2H_6/C_2H_4$  (1/1, v/v, 2 mL  $\text{min}^{-1}$ ) mixtures at 298 K.

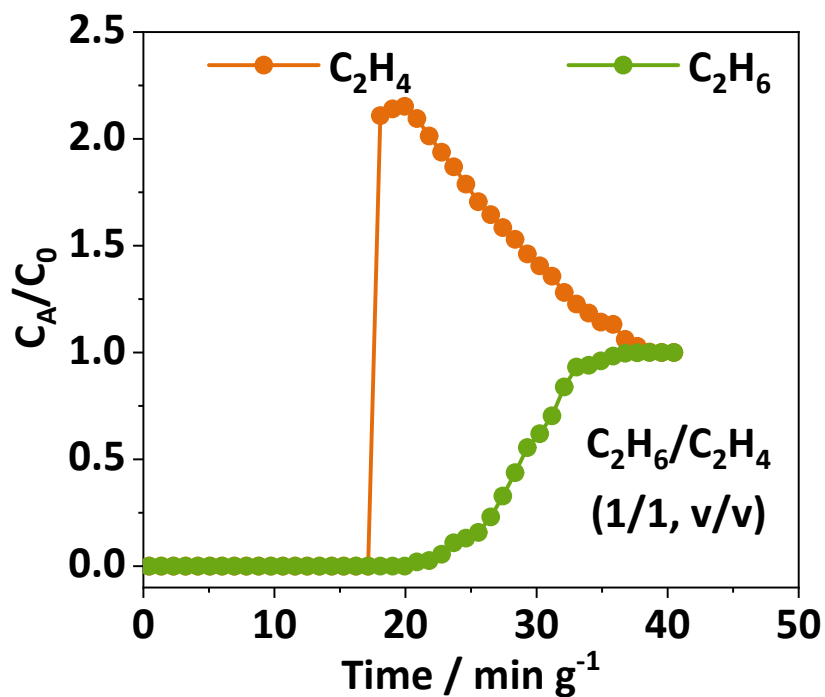


Figure S69. Experimental breakthrough curves of NTU-73-CH<sub>3</sub> for C<sub>2</sub>H<sub>6</sub>/C<sub>2</sub>H<sub>4</sub> (1/1, v/v, 2 mL min<sup>-1</sup>) mixtures at 298 K.

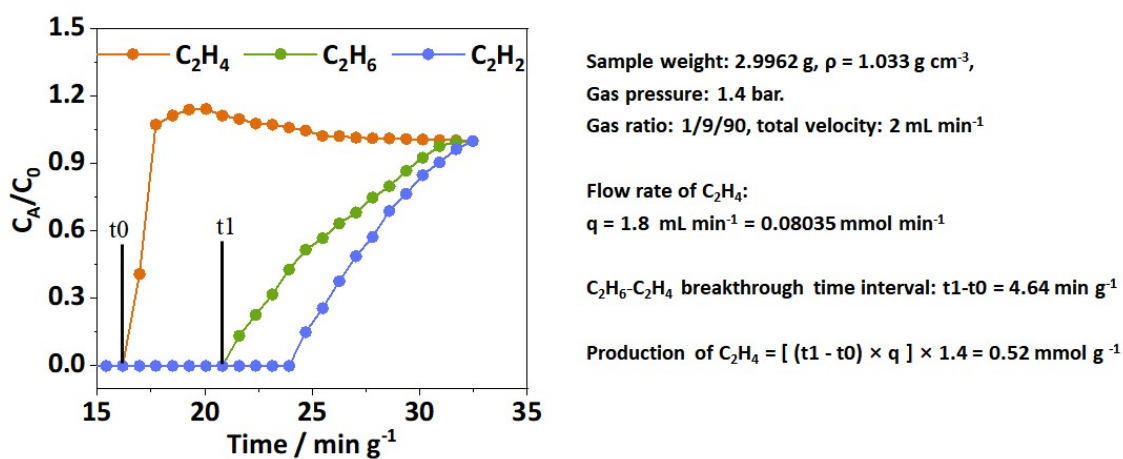


Figure S70. Production of C<sub>2</sub>H<sub>4</sub> during C<sub>2</sub> breakthrough process in NTU-73-CH<sub>3</sub> at 298K.

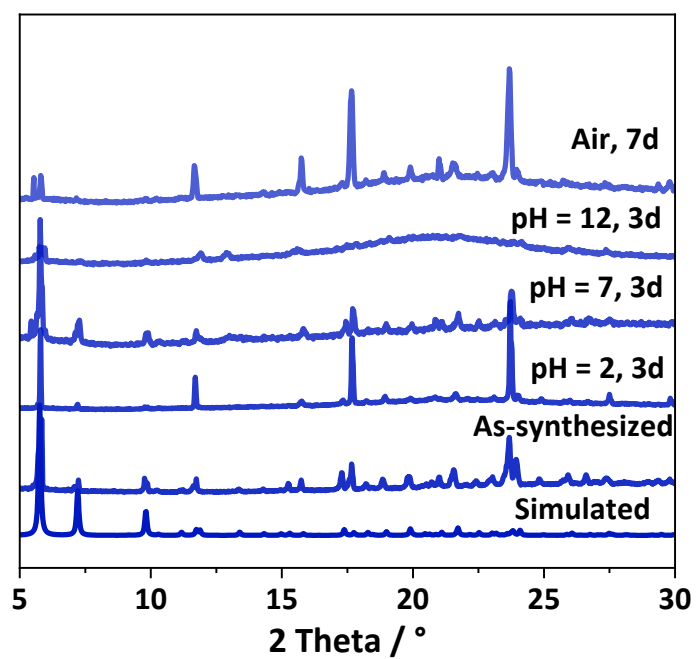


Figure S71. PXRD patterns of NTU-73-COOH after exposure to chemical solutions and air.

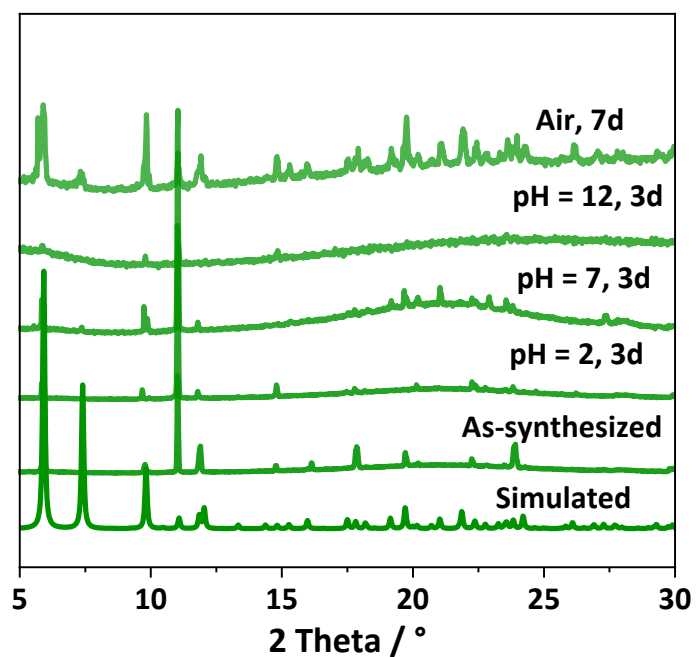


Figure S72. PXRD patterns of NTU-73-CF<sub>3</sub> after exposure to chemical solutions and air.

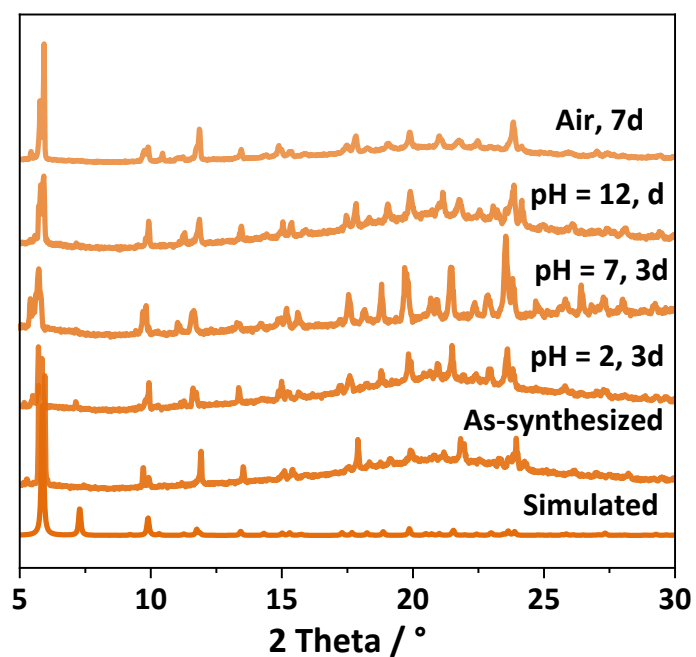


Figure S73. PXRD patterns of NTU-73-CH<sub>3</sub> after exposure to chemical solutions and air.

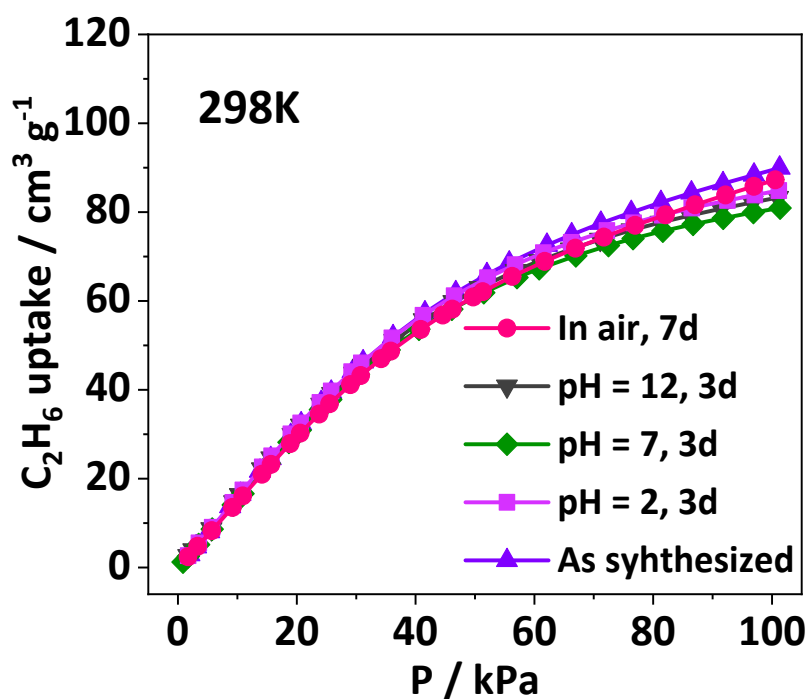


Figure S74. C<sub>2</sub>H<sub>6</sub> adsorption isotherms of treated NTU-73-CH<sub>3</sub> at 298 K.

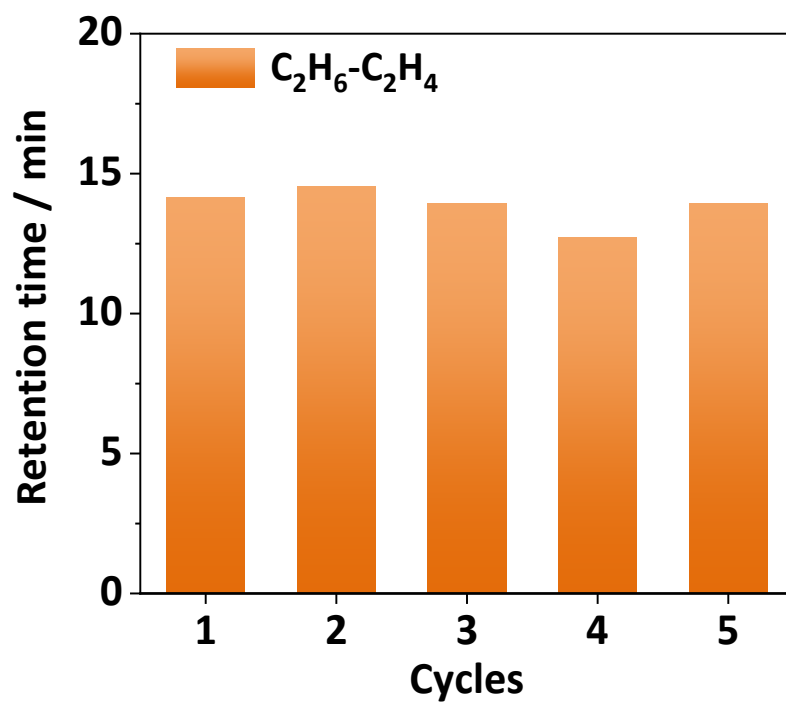


Figure S75. Retention time of cycling breakthrough experiments of NTU-73-CH<sub>3</sub> for C<sub>2</sub>H<sub>6</sub>/C<sub>2</sub>H<sub>4</sub> mixture (1/9, v/v) at 298 K.

**Table S1.** Single crystal data of **NTU-73-COOH**, **NTU-73-CF<sub>3</sub>** and **NTU-73-CH<sub>3</sub>**.

	<b>NTU-73-COOH</b>	<b>NTU-73-CF<sub>3</sub></b>	<b>NTU-73-CH<sub>3</sub></b>
Empirical formula	C <sub>26</sub> H <sub>20</sub> Cu <sub>2</sub> F <sub>6</sub> N <sub>8</sub> O <sub>4</sub> Zr	C <sub>26</sub> H <sub>18</sub> CuF <sub>12</sub> N <sub>8</sub> Zr	C <sub>26</sub> H <sub>24</sub> CuF <sub>6</sub> N <sub>8</sub> Zr
Formula weight	777.27	825.25	717.30
Space group	I4 <sub>1</sub> 22	I4 <sub>1</sub> 22	I4 <sub>1</sub> 22
<i>a</i> / Å	16.848 (5)	16.8824 (16)	17.1374 (9)
<i>b</i> / Å	16.848 (5)	16.8824 (16)	17.1374 (9)
<i>c</i> / Å	31.093 (17)	31.921(6)	31.400 (3)
Crystal System	tetragonal	tetragonal	tetragonal
<i>V</i> / Å <sup>3</sup>	8826 (7)	9098 (2)	9221.9 (13)
Z	8	8	8
Density / g cm <sup>-3</sup>	1.170	1.205	1.033
Index ranges	-21 ≤ <i>h</i> ≤ 21 -21 ≤ <i>k</i> ≤ 20 -40 ≤ <i>l</i> ≤ 40	-20 ≤ <i>h</i> ≤ 20 -20 ≤ <i>k</i> ≤ 19 -38 ≤ <i>l</i> ≤ 38	-20 ≤ <i>h</i> ≤ 20 -20 ≤ <i>k</i> ≤ 19 -37 ≤ <i>l</i> ≤ 37
<i>R</i> <sub>1</sub>	0.0583	0.0409	0.033
<i>wR</i> <sub>2</sub> [ <i>I</i> > 2σ ( <i>I</i> )]	0.1283	0.1338	0.0930
F (000)	3096	3256	2872.0
GOOF	1.041	1.064	1.072

$$R = \sum ||F_o| - |F_c|| / \sum |F_o|, wR = \{\sum[w(|F_o|^2 - |F_c|^2)^2] / \sum[w(|F_o|^4)]\}^{1/2} \text{ and } w = 1 / [\sigma^2(F_o^2) + (0.1452P)^2] \text{ where } P = (F_o^2 + 2F_c^2) / 3$$

**Table S2.** Summarized the CO<sub>2</sub> uptake at 195 K, the calculated pore size, BET surface area and pore volume.

PCPs	Uptake (cm <sup>3</sup> g <sup>-1</sup> )	Pore size (Å)	BET (m <sup>2</sup> g <sup>-1</sup> )	Volume (m <sup>3</sup> g <sup>-1</sup> )
<b>NTU-73-COOH</b>	62.983	5.3	228.28	0.039
<b>NTU-73-CF<sub>3</sub></b>	194.42	7.7	888.89	0.153
<b>NTU-73-CH<sub>3</sub></b>	250.2	9.2	1077.6	0.185

**Table S3.** Summarized performance of ternary C2 hydrocarbon separation toward reported materials.

PCPs	C <sub>2</sub> H <sub>2</sub> uptake	C <sub>2</sub> H <sub>4</sub> uptake	C <sub>2</sub> H <sub>6</sub> uptake	Selectivity of C <sub>2</sub> H <sub>2</sub> /C <sub>2</sub> H <sub>4</sub> 1:99	Selectivity of C <sub>2</sub> H <sub>6</sub> /C <sub>2</sub> H <sub>4</sub> 1:1	C <sub>2</sub> H <sub>6</sub> and C <sub>2</sub> H <sub>4</sub> uptake difference	Production of pure C <sub>2</sub> H <sub>4</sub> (Feed gas ratio: v/v/v)	Refs
LIFM-XYX-7	108.90	91.20	117.20	1.24	1.50	26.00	/	5
NPU-3	56.90	49.06	74.59	1.32 <sup>d</sup>	3.21	25.53	/	6
UiO-67-(NH <sub>2</sub> ) <sub>2</sub>	132.16	96.77	119.17	2.10	1.70	22.40	0.55 (1/49.5/49.5)	7
NPU-2	89.38	76.61	99.01	1.25 <sup>d</sup>	1.52	22.40	/	6
Azole-Th-1	81.20	81.10	100.20	1.09 <sup>d</sup>	1.46	19.10	1.34 (1/9/90)	8
MOF-808-Bzz	66.75	32.03	49.28	3.15	1.90	17.25	/	9
UPC-612	67.44	62.58	80.11	1.07 <sup>e</sup>	1.40	17.53	0.47 (1/1/1)	10
Al-PyDC	184.58 <sup>b</sup>	77.06 <sup>b</sup>	94.08 <sup>b</sup>	4.30 <sup>b</sup>	1.90 <sup>b</sup>	17.02	1.61 (1/9/90)	11
LIFM-XYX-6	66.50	50.10	66.90	1.53	1.63	16.80	0.14 (1/9/90)	5
Zn(ad)(int)	33.40 <sup>c</sup>	26.25 <sup>c</sup>	41.00 <sup>c</sup>	1.61	2.40	14.75	1.43 (1/10/89)	12
NTU-73-CH <sub>3</sub>	98.02	77.81	89.92	3.23	1.33	12.11	0.52 (1/9/90)	This work
ZJNU-115	106.00	84.00	94.20	2.05	1.56	10.20	/	13
CuTiF <sub>6</sub> -TPPY	81.09	54.21	63.17	5.03	2.12 <sup>g</sup>	8.96	/	14
UPC-66-a	71.30 <sup>a</sup>	54.00 <sup>a</sup>	61.90 <sup>a</sup>	1.05 <sup>a, d</sup>	1.65 <sup>a, d</sup>	7.90	2.01 (1/1/89)	15
MIL-160	204.29	96.32	104.16	2.06 <sup>d</sup>	1.58	7.84	0.21 (1/1/1)	16
Zn-(BDC)(H <sub>2</sub> BPZ)]	100.00	73.60	81.00	1.60	2.20	7.40	0.21 (3/3/10)	17
ZJNU-7	112.80	85.20	92.50	1.77	1.58	7.30	/	18
NPU-1	114.24	94.08	100.8	1.40 <sup>d</sup>	1.32	6.72	/	6
TJT-100	99.90	77.06	82.88	1.80	1.20 <sup>f</sup>	5.82	0.41 (1/1/98)	19
NUM-9a	52.10	49.90	55.55	1.48	1.61 <sup>g</sup>	5.65	/	20
UPC-613	63.40	51.70	57.10	1.39 <sup>e</sup>	1.50	5.40	/	10
Ni(sdba)(dabco) <sub>0.5</sub>	98.78	66.98	70.56	2.28 <sup>d</sup>	2.47	3.58	0.83 (1/9/90)	21
CAU-23	123.76	92.96	96.32	10.65 <sup>d</sup>	1.64	3.36	0.18 (1/1/1)	16
Zn-ATA	17.92 <sup>c</sup>	15.01 <sup>c</sup>	17.92 <sup>c</sup>	1.81	1.84	2.90	0.72 (1/10/89)	22
NTU-73-CF <sub>3</sub>	77.74	62	62.68	2.52	1.17	0.68	0.30 (1/9/90)	This work
Zn-atz-oba	62.00	45.20	45.70	1.43 <sup>d</sup>	1.27	0.50	/	23
MOF-303	177.86	112.50	112.00	2.40	1.70	-0.50	1.35 (1/9/90)	24
NTU-73-COOH	32.34	12.97	11.82	29.52	0.66	-1.15	/	This work

Note: a: 293 K.; b: 296 K; c: 0.1 bar; d: C<sub>2</sub>H<sub>2</sub>/C<sub>2</sub>H<sub>4</sub> = 1/1 (v/v); e: C<sub>2</sub>H<sub>2</sub>/C<sub>2</sub>H<sub>4</sub> = 1/9 (v/v); f: C<sub>2</sub>H<sub>6</sub>/C<sub>2</sub>H<sub>4</sub> = 1/99 (v/v); g: C<sub>2</sub>H<sub>6</sub>/C<sub>2</sub>H<sub>4</sub> = 1/9 (v/v).

**Table S4.** Summarized performance based C<sub>2</sub>H<sub>6</sub>-C<sub>2</sub>H<sub>4</sub> uptake difference (> 10 cm<sup>3</sup> g<sup>-1</sup>) toward reported materials.

PCPs	C <sub>2</sub> H <sub>2</sub> uptake	C <sub>2</sub> H <sub>4</sub> uptake	C <sub>2</sub> H <sub>6</sub> uptake	Selectivity of C <sub>2</sub> H <sub>2</sub> /C <sub>2</sub> H <sub>4</sub> 1:99	Selectivity of C <sub>2</sub> H <sub>6</sub> /C <sub>2</sub> H <sub>4</sub> 1:1	C <sub>2</sub> H <sub>6</sub> and C <sub>2</sub> H <sub>4</sub> uptake difference	Production of pure C <sub>2</sub> H <sub>4</sub> (Feed gas ratio: v/v/v)	Refs
Al-PyDC	184.58 <sup>a</sup>	77.06 <sup>a</sup>	94.08 <sup>a</sup>	4.3 <sup>a</sup>	1.90 <sup>a</sup>	17.02	1.61 (1/9/90)	11
<b>NTU-73-CH<sub>3</sub></b>	<b>98.02</b>	<b>77.81</b>	<b>89.92</b>	<b>3.23</b>	<b>1.33</b>	<b>12.11</b>	<b>0.52 (1/9/90)</b>	<b>This work</b>
MOF-808-Bzz	66.75	32.03	49.28	3.15	1.90	17.25	/	9
UiO-67-(NH <sub>2</sub> ) <sub>2</sub>	132.16	96.77	119.17	2.1	1.70	22.40	0.55 (1/49.5/49.5)	7
ZJNU-115	106.00	84.00	94.20	2.05	1.56	10.20	/	13
Zn(ad)(int)	33.40 <sup>b</sup>	26.25 <sup>b</sup>	41.00 <sup>b</sup>	1.61	2.40	14.75	1.43 (1/10/89)	12
LIFM-XYX-6	66.50	50.10	66.90	1.53	1.63	16.80	0.14 (1/9/90)	5
NPU-3	56.90	49.06	74.59	1.32 <sup>c</sup>	3.21	25.53	/	6
NPU-2	89.38	76.61	99.01	1.25 <sup>c</sup>	1.52	22.40	/	6
LIFM-XYX-7	108.90	91.20	117.20	1.24	1.50	26.00	/	5
Azole-Th-1	81.20	81.10	100.20	1.09 <sup>c</sup>	1.46	19.10	1.34 (1/9/90)	8
UPC-612	67.44	62.58	80.11	1.07 <sup>d</sup>	1.40	17.53	0.47 (1/1/1)	10

Note: a: 296 K; b: 0.1 bar. c: C<sub>2</sub>H<sub>2</sub>/C<sub>2</sub>H<sub>4</sub> = 1/1 (v/v). d: C<sub>2</sub>H<sub>2</sub>/C<sub>2</sub>H<sub>4</sub> = 1/9 (v/v).

**Table S5.** Single crystal data of  $C_2H_4\supset NTU-73-COOH$ ,  $C_2H_6\supset NTU-73-COOH$ ,  $C_2H_4\supset NTU-73-CF_3$ ,  $C_2H_6\supset NTU-73-CF_3$ ,  $C_2H_4\supset NTU-73-CH_3$  and  $C_2H_6\supset NTU-73-CH_3$ .

	$C_2H_4\supset NTU-73-COOH$	$C_2H_6\supset NTU-73-COOH$	$C_2H_4\supset NTU-73-CF_3$	$C_2H_6\supset NTU-73-CF_3$	$C_2H_4\supset NTU-73-CH_3$	$C_2H_6\supset NTU-73-CH_3$
Empirical formula	$C_{26}H_{20}CuF_6N_8O_4Zr, 0.5C_2H_4$	$C_{26}H_{20}CuF_6N_8O_4Zr, 0.5C_2H_6$	$C_{26}H_{18}CuF_{12}N_8Zr, 1.5C_2H_4$	$C_{26}H_{18}CuF_{12}N_8Zr, 1.5C_2H_6$	$C_{26}H_{24}CuF_6N_8Zr, 2.5C_2H_4$	$C_{26}H_{24}CuF_6N_8Zr, 2.5C_2H_6$
Formula weight	793.30	794.30	867.33	870.25	787.30	792.30
Space group	$I4_122$	$I4_122$	$I4_122$	$I4_122$	$I4_122$	$I4_122$
$a / \text{Å}$	17.105 (3)	16.9799 (5)	16.7225 (5)	16.8758 (2)	17.0131 (3)	16.9122 (7)
$b / \text{Å}$	17.105 (3)	16.9799 (5)	16.7225 (5)	16.8758 (2)	17.0131 (3)	16.9122 (7)
$c / \text{Å}$	31.249 (11)	31.1337 (11)	31.8580 (14)	31.7415 (11)	31.4540 (13)	31.516 (3)
Crystal System	tetragonal	tetragonal	tetragonal	tetragonal	tetragonal	tetragonal
$V / \text{Å}^3$	9143 (5)	8976.4 (6)	8908.8 (7)	9039.8 (4)	9104.2 (5)	9014.3 (11)
Z	8	8	8	8	8	8
Density / $\text{g cm}^{-3}$	1.201	1.228	1.293	1.282	1.033	1.135
Index ranges	$-22 \leq h \leq 22$ $-22 \leq k \leq 21$ $-40 \leq l \leq 40$	$-22 \leq h \leq 22$ $-22 \leq k \leq 21$ $-40 \leq l \leq 40$	$-20 \leq h \leq 20$ $-22 \leq k \leq 21$ $-39 \leq l \leq 39$	$-20 \leq h \leq 20$ $-22 \leq k \leq 21$ $-39 \leq l \leq 39$	$-20 \leq h \leq 20$ $-20 \leq k \leq 19$ $-38 \leq l \leq 38$	$-20 \leq h \leq 20$ $-20 \leq k \leq 19$ $-38 \leq l \leq 38$
$R_1$	0.0662	0.0562	0.0713	0.0356	0.0440	0.0447
$wR_2 [I > 2\sigma(I)]$	0.2120	0.1769	0.1967	0.1035	0.1440	0.1323
F (000)	3320.0	3348.0	3448.0	3472.0	3096.0	3124.0
GOOF	1.116	1.192	1.347	1.169	1.182	1.127

$$R = \sum ||F_o| - |F_c|| / \sum |F_o|, wR = \{\sum [w(|F_o|^2 - |F_c|^2)^2] / \sum [w(|F_o|^4)]\}^{1/2} \text{ and } w = 1 / [\sigma^2(F_o^2) + (0.1452P)^2] \text{ where } P = (F_o^2 + 2F_c^2) / 3$$

## References

- 1 Y. F. Duan, Y. H. Huang, C. Q. Wang, Q. Wang, K. Ge, Z. Y. Lu, H. J. Wang, J. G. Duan, J. F. Bai and W. Q. Jin, *Chem. Sci.*, 2023, **14**, 4605-4611.
- 2 G. M. Sheldrick, *Acta Crystallogr. A*, 2008, **64**, 112-122.
- 3 P. Vandersluis and A. L. Spek, *Acta Crystallogr. A*, 1990, **46**, 194-201.
- 4 A. L. Spek, *J. Appl. Crystallogr.*, 2003, **36**, 7-13.
- 5 Y. Y. Xiong, C.-X. Chen, T. Pham, Z.-W. Wei, K. A. Forrest, M. Pan and C. Y. Su, *CCS Chem.*, 2023, **6**, 241-254.
- 6 B. Y. Zhu, J. W. Cao, S. Mukherjee, T. Pham, T. Zhang, T. Wang, X. Jiang, K. A. Forrest, M. J. Zaworotko and K. J. Chen, *J. Am. Chem. Soc.*, 2021, **143**, 1485-1492.
- 7 X. W. Gu, J. X. Wang, E. Y. Wu, H. Wu, W. Zhou, G. D. Qian, B. L. Chen and B. Li, *J. Am. Chem. Soc.*, 2022, **144**, 2614-2623.
- 8 Z. Xu, X. Xiong, J. Xiong, R. Krishna, L. Li, Y. Fan, F. Luo and B. Chen, *Nat. Commun.*, 2020, **11**, 3163-3172.
- 9 C. Song, F. Zheng, Y. Liu, Q. Yang, Z. Zhang, Q. Ren and Z. Bao, *Angew. Chem. Int. Ed.*, 2023, **62**, e202313855.
- 10 Y. T. Wang, C. L. Hao, W. D. Fan, M. Y. Fu, X. K. Wang, Z. K. Wang, L. Zhu, Y. Li, X. Q. Lu, F. N. Dai, Z. X. Kang, R. M. Wang, W. Y. Guo, S. Q. Hu and D. F. Sun, *Angew. Chem. Int. Ed.*, 2021, **60**, 11350-11358.
- 11 E. Wu, X.-W. Gu, D. Liu<sup>1</sup>, X. Zhang, HuiWu, W. Zhou, G. Qian and B. L. 1, *Nat. Commun.*, 2023, **14**, 6146-6157.
- 12 Q. Ding, Z. Zhang, Y. Liu, K. Chai, R. Krishna and S. Zhang, *Angew. Chem. Int. Ed.*, 2022, **61**, e202208134.
- 13 L. Fan, P. Zhou, X. Wang, L. Yue, L. Li and Y. He, *Inorg. Chem.*, 2021, **60**, 10819-10829.
- 14 P. Zhang, Y. Zhong, Y. Zhang, Z. Zhu, Y. Liu, Y. Su, J. Chen, S. Chen, Z. Zeng, H. Xing, S. Deng and J. Wang, *Sci. Adv.*, 2022, **8**, eabn9231.
- 15 Y. Wang, M. Fu, S. Zhou, H. Liu, X. Wang, W. Fan, Z. Liu, Z. Wang, D. Li, H. Hao, X. Lu, S. Hu and D. Sun, *Chem*, 2022, **8**, 3263-3274.
- 16 S. Xian, J. Peng, H. Pandey, W. Graham, L. Yu, H. Wang, K. Tan, T. Thonhauser and J. Li, *J. Mater. Chem. A*, 2023, **11**, 21401-21410.
- 17 G. D. Wang, Y. Z. Li, W. J. Shi, L. Hou, Y. Y. Wang and Z. Zhu, *Angew. Chem. Int. Ed.*, 2022, **61**, e202205427.
- 18 Z. Jiang, L. Fan, P. Zhou, T. Xu, S. Hu, J. Chen, D. L. Chen and Y. He, *Inorg. Chem. Front.*, 2021, **8**, 1243-1252.
- 19 H. G. Hao, Y. F. Zhao, D. M. Chen, J. M. Yu, K. Tan, S. Q. Ma, Y. Chabal, Z. M. Zhang, J. M. Dou, Z. H. Xiao, G. Day, H. C. Zhou and T. B. Lu, *Angew. Chem. Int. Ed.*, 2018, **57**, 16067-16071.
- 20 S. Q. Yang, F.-Z. Sun, P. Liu, L. Li, R. Krishna, Y.-H. Zhang, Q. Li, L. Zhou and T.-L. Hu, *ACS Appl. Mater. Interfaces*, 2020, **13**, 962-969.
- 21 H. Shuai, J. Liu, Y. Teng, X. Liu, L. Wang, H. Xiong, P. Wang, J. Chen, S. Chen, Z. Zhou, S. Deng and J. Wang, *Sep. Purif. Technol.*, 2023, **323**, 124392.
- 22 Q. Ding, Z. Zhang, P. Zhang, C. Yu, C. H. He, X. Cui and H. Xing, *Chem. Eng. J.*, 2022, **450**, 138272.
- 23 J. W. Cao, S. Mukherjee, T. Pham, Y. Wang, T. Wang, T. Zhang, X. Jiang, H.-J. Tang, K. A. Forrest, B. Space, M. J. Zaworotko and K.-J. Chen, *Nat. Commun.*, 2021, **12**, 6507-6515.
- 24 H. M. Wen, C. Yu, M. Liu, C. Lin, B. Zhao, H. Wu, W. Zhou, B. Chen and J. Hu, *Angew. Chem. Int. Ed.*, 2023, **62**, e202309108.